



## A comprehensive study of the tides around the Welsh coastal waters

J.M. Horrillo-Caraballo<sup>a</sup>, Y. Yin<sup>b</sup>, I. Fairley<sup>a</sup>, H. Karunaratna<sup>a</sup>, I. Masters<sup>a</sup>, D.E. Reeve<sup>a,\*</sup>

<sup>a</sup> Zienkiewicz Centre for Computational Engineering, Swansea University, Bay Campus, Fabian Way, Swansea, SA1 8EN, Wales, UK

<sup>b</sup> Leibniz-Institute for Baltic Sea Research, Warnemünde, Seestrasse 15, D-18119 Rostock, Germany

### ARTICLE INFO

#### Keywords:

Tides  
Computational model  
Welsh coastal waters  
Residual currents  
Shallow water harmonics  
Vorticity

### ABSTRACT

A computational model has been used to explore characteristics of the barotropic tide around the Welsh coast in detail for the first time. Proper understanding of tidal characteristics is vital for the sustainable use of marine resources; particularly for industries such as marine energy extraction, aggregate mining, aquaculture, as well as regulators and agencies with responsibilities for the resource management and public safety. In shallow water areas, the influence of bathymetry and energy dissipation leads to the generation of higher harmonics that cause complex tidal phenomena. The Celtic and Irish seas, which enclose the Welsh coast (UK), are heavily industrialised shallow water seas with macro-to mega-tidal semi-diurnal tides. It is shown that tidal distortion is significant in the Bristol Channel (S. Wales) and in the large shallow estuaries of the N. Wales coast; for much of the west coast this is only significant in localised areas around headlands and islands. Tidal dominance switches from flood dominant in the south and north to ebb dominant on the west coast. Highly complex patterns of vorticity in the tidal residual flow are noted. All these factors mean that careful siting of industry and coastal management interventions is required to avoid disruption of the natural system.

### 1. Introduction

One of the major challenges for coastal engineers and coastal managers is addressing the risk of coastal flooding. Less visible but of similar importance are the changes in seabed morphology due to sediment transport by waves and tides. Such changes may alter both the flood risk but also the sustainability of ports and harbours, as well as threatening the ecology of environmentally important coastal sites, (Environment Agency, 2021). An understanding of the tidal variations in sea level and currents is an important element in planning coastal defence, shoreline management strategies and siting of marine energy extraction. Potential exists for both tidal stream energy projects, (Bryden and Couch, 2006), that extract energy from the tidal flow, and tidal range projects that generate energy from the variation in potential energy provided by high tidal range, (Neill et al., 2018). Further, it has been suggested that large projects such as the Severn Barrage would modify the flows to an extent that the performance of distant tidal energy schemes might be compromised, (Willis et al. (2010)). The primary strategy for resolving potential conflicts across the range of interests in using the seas is Marine Spatial Planning, a recent example of this within the region of interest is the Wales National Marine Plan (Welsh Government, 2019). Marine and shoreline plans require consistency and one of the main

elements linking the two are the tides.

The tide generating forces arise from the differential gravitational attraction of the Moon and Sun experienced over the surface of the Earth. The oceans respond dynamically to these forces and interact with the irregular seabed and continents to create a complex and changing pattern of interference, or amphidromic systems. As a stratified fluid the ocean can support both external (barotropic) and internal (baroclinic) tides. With the exception of some highly stratified situations, the barotropic tides contribute most to the rise and fall of the sea surface and provide a very good approximation to the measured tidal level variations, (Cummins and Oey, 1997), and are the focus of this paper. Navigation, aquaculture and flood defence interests all require information on the daily variation of tide levels and currents. However, longer term tidal influences, arising from the cumulative effect of small asymmetries in the tidal oscillation, can have significant impacts on pollutant transport and sediment movements, (e.g. Prandle, 1984; McCave, 1970).

There is a vast literature on deep ocean tides and their propagation into shallower shelf seas. Tides around continents often have amplified magnitudes in relation to deep ocean tides. Fluid bodies forced by oscillations close to their natural frequency can have a large amplitude response; a process called resonance (Pugh, 1981), which occurs when the continental shelf is  $\frac{1}{4}$  wavelength wide. A similar process can occur

\* Corresponding author.

E-mail address: [d.e.reeve@swansea.ac.uk](mailto:d.e.reeve@swansea.ac.uk) (D.E. Reeve).

<https://doi.org/10.1016/j.ecss.2021.107326>

Received 17 September 2020; Received in revised form 4 March 2021; Accepted 5 March 2021

Available online 19 March 2021

0272-7714/© 2021 The Authors. Published by Elsevier Ltd. This is an open access article under the CC BY license (<http://creativecommons.org/licenses/by/4.0/>).

at a constriction of the sea, such as the English Channel, the Bristol Channel or the northern end of the Irish Sea. An exactly analogous situation exists at smaller scale when long waves encounter the entrance of an inlet or harbour. In the case of estuaries the amplification of the tidal oscillation is explained by shoaling caused by the decrease in water depth, and funnelling due to geographic constriction of the wave front. In the idealised case of no frictional losses, conservation of the tidal energy flux along a channel implies amplification of the tide progressing up a channel according to Green's law, (Jay 1991). Resonance, *per se*, requires reflection of the incoming wave and constructive interference between incoming and reflected wave. In harbours reflection is caused by the hard walls and breakwaters; in engineered estuaries it may be a barrier or weir that restricts the propagation of the tidal wave; and in natural estuaries reflection may occur due to a rapid change in bed level at the transition from flood plain to tidal river. Vigorous tidal motions in shelf seas arise from resonance with ocean tides and from local amplification due to the seabed configuration rather than direct action from the tide generating forces, (Pingree and Griffiths, 1987; Kang et al., 1998). This amplification can be dramatic in funnel shaped and resonant channels, as in the case of the Bay of Fundy (Canada) and the Bristol Channel (UK) where the maximum spring tidal range can exceed 14 m. The tides around the Welsh coast are highly amplified, in some locations being classified as mega-tidal; where the tidal range is in excess of 8 m.

Tidal amplification is modified by frictional momentum dissipation and nonlinear interactions that distort the sinusoidal character of the deep ocean tides and generate shallow water harmonics: overtides which have frequencies that are multiples of those of the basic astronomical constituents, for instance  $M_4$  that has a frequency twice that of  $M_2$ ; and compound tides which arise through interactions of two different harmonics, for instance  $MS_4$  that has a frequency equal to the sum of those of  $M_2$  and  $S_2$ , (see e.g. Aubrey and Speer, 1985; Friedrichs and Aubrey, 1988). An important consequence of tidal wave distortion is the asymmetry of tidal motion in shallow water: the periods of tidal rise and tidal fall may not be equal; the magnitude and duration of flood and ebb tidal flows may be unequal, (Gallo and Vinzon, 2005). This asymmetry can lead to preferential transport of sediments by the tidal oscillation either into or out of an estuary. Understanding tidal asymmetry is important from the marine renewable perspective too, as high tidal asymmetry can adversely affect tidal power extraction due to the high dominance of either an ebb or flood flow, (Neill et al., 2014; Ward et al., 2018). Further, Neill et al. (2009) demonstrated that tidal energy extraction can modify the hydrodynamics of a region and in areas of high non-linearity may have significant consequences for the dynamics of sediments due to the generation of residual flows.

Asymmetry in the tidal oscillation leads to a net drift or tidal residual current. Sediment transport is widely considered to obey a power law with respect to the tidal velocity, (e.g. Lavelle et al., 1984; Van Rijn, 1993). The quasi-oscillatory nature of tidal currents suggests net sediment movement due to tidal currents might be in the direction of the residual current direction. This perspective is supported by the correlation of tidal residual currents with long term sediment movements, (see e.g. McCave, 1970; De Swart and Zimmerman, 2009; Moore et al., 2009).

The origin of tidal asymmetries is through non-linear dynamics such as advection and bed shear stress. Although tidal forcing at the mouth of an estuary or embayment is often at diurnal or semi-diurnal frequencies, the nonlinear terms in the momentum equations almost always produce significant higher harmonics in shallow water (Aubrey and Speer, 1985). Ianniello (1979) showed that while first-order tidal propagation is relatively insensitive to small bathymetric variations the associated nonlinearities result in the generation of significant higher harmonic and residual components, with frictional effects being pronounced in strongly convergent channels, irrespective of depth, (Friedrichs and Aubrey, 1994). Tidal asymmetries are very often associated with the quarter-diurnal tidal component,  $M_4$ , which tends to be more pronounced in locations where the coastal zone is shallow and the tidal

amplitude is large, (Song et al., 2011). This may be understood in a simple way from the trigonometric relationship

$$U_1 \cos(\omega_1 t) \times U_2 \cos(\omega_2 t) = \frac{U_1 U_2}{2} \{ \cos(\omega_1 - \omega_2)t + \cos(\omega_1 + \omega_2)t \} \quad (1)$$

in which the product of two harmonics of frequencies  $\omega_1$  and  $\omega_2$  and amplitudes  $U_1$  and  $U_2$  results in constituents at their sum and difference frequencies. Thus, terms involving the product of the  $M_2$  harmonic generate both  $M_4$  and  $Z_0$  harmonics; an overtide and a residual (constant). Similarly,  $M_2$  and  $S_2$  will generate  $\omega_1 + \omega_2 = \omega_{MS2}$  and  $\omega_2 - \omega_1 = \omega_{MS6}$ , that is, quarter-diurnal and fortnightly periods. In fact, as discussed in Prandle (2009), the advective terms act in this manner but the quadratic friction term generates odd harmonics (i.e.  $M_6$  and  $M_{10}$  from  $M_2$ ) as well as  $M_4$ . These harmonics play a crucial part in the seabed sediment dynamics and in the net transport of pollutants (Pingree and Griffiths, 1979). They are also sensitive to the details of the local bathymetry and can be difficult to predict with traditional methods, (Adcock and Draper, 2014). The practical application of such theory is illustrated by the study of Shapiro (2011) who showed that tidal power extraction may affect the residual circulation as far as 100 km away from its location.

Here, a distinction is made between the residual (of either elevation or current) obtained by an harmonic analysis of tide gauge records and the residual obtained from a computational simulation of tidal flow. The former will likely contain contributions from non-tidal sources such as waves, surface pressure and surface winds. The latter arise solely due to asymmetries in the tidal flows caused by nonlinear interactions and bathymetric configuration, and are termed tidal residuals henceforward.

Modelling studies by Prandle (1978, 1984) showed typical tidal residual currents of 1–3 cm/s over the continental shelf around the UK. Tidal residual currents are usually much smaller than flood or ebb currents but their significance to sediment movement should be viewed from the perspective of their action over many months or years. Maps of residual currents often reveal the presence of closed circulation cells or 'gyres' that can act to trap mobile sediment, (e.g. Takasugi et al., 1994). The existence of gyres can be understood as a transfer of vorticity from the fluctuating tidal motion to the mean (residual) field, (Robinson, 1983). The most important vorticity generation mechanism is the squeezing and stretching of the water column over the sea topography (Zimmerman, 1981), while the torque from the bottom friction force may also be significant, (Robinson, 1983; Ridderinkhof, 1989). The vorticity provides a quantitative measure of the strength of gyres in the residual flow.

Zimmerman (1981) argued from theoretical considerations that while bottom morphology influenced the residual currents there were also feedbacks from the residual currents in altering the bottom morphology. This is important in areas with morphological features composed of mobile sediment (e.g. sandbanks and sand waves), in which residual currents will shape the sandbanks and at the same time the sandbanks will shape the residual current flow. An explanation for the growth and maintenance of sandbanks in terms of residual currents was provided by Huthnance (1982) and subsequently expanded to explain the movement of sandwaves, (Hulscher et al., 1993). As noted by Van Veelen et al. (2018) in their study of sandbank evolution, the evolution of the seabed follows from the tidally averaged bed load sediment transport, which is directly related to the tidal residual currents. Indeed, studies of the historical evolution of the Gt. Yarmouth sandbanks (Horrillo-Caraballo and Reeve, 2008) and sandbanks in the Pentland Firth (Chatzirodou et al., 2017) have confirmed the importance of this feedback mechanism in coastal morphodynamics. From this perspective, the analysis and interpretation of tidal residuals with respect to a single snapshot of bathymetry, especially one that is composed of mobile sediments, is best seen as a diagnostic tool rather than a reliable prognostic technique.

Doodson et al. (1954) developed one of the earliest computational

models of tides in the Irish Sea simulating the propagation of the  $M_2$  tide and validated their results against the observations of Doodson and Corkan (1932). Subsequently, Robinson (1979) produced cotidal maps for the main constituents ( $M_2$ ,  $S_2$ ,  $N_2$ ,  $O_1$ ,  $K_1$ ) and some shallow water constituents using current meter measurements of the area of the Irish Sea. One of the first computational models of the North-west European continental shelf was presented by Flather (1976). Modelling capabilities improved rapidly in the following decades as computer speeds and computational modelling techniques evolved. Davies (1986) and Davies and Jones (1992) considered three-dimensional effects in their model of main constituent tides in the Irish and Celtic Sea, which was based on a vertical eddy viscosity parameterisation technique. Results were improved by Aldridge and Davies (1993) and Davies and Aldridge (1993) with higher resolution grids and by Gekeler (1995) who incorporated data assimilation into a 3-D finite difference model of tides in the Irish Sea. While Jones and Davies (2007) investigated the contributions of the five main tidal constituents plus the overtides  $M_4$  and  $M_6$  using a finite element model, concluding that it was necessary to include shallow water harmonics to achieve good accuracy in the tidal elevations and currents. The asymmetry of the tidal variation can have significant implications on the efficiency of tidal stream energy extraction, as argued by Neill et al. (2014), as the power output is related to the velocity cubed, which means that small changes in asymmetry in the velocity will have a large effect on the power output. Additionally, construction of tidal energy infrastructure such as tidal barrages has the potential to alter the larger scale tidal propagation characteristics, (Zhou et al., 2014). The preponderance of studies has concentrated either on the Liverpool Bay area or on the Severn Estuary or in small areas suitable for marine energy device deployments. Areas such as Cardigan Bay have received little attention; in general, the tidal dynamics around the Welsh coast has not been studied as in an integrated and coherent manner.

In this study, a hydrodynamic model of the Irish and Celtic Sea has been configured to investigate the barotropic tidal dynamics and the effects of the non-linearity of the tides (compound tides and overtides) around the coast of Wales. The effects of stratification on tides have been noted in localised regions within this domain, (e.g. Pingree, 1980), but are not considered in this paper. The model employed is Delft3D which was configured to run for depth-averaged flow. The tidal flows were driven by 13 constituents along its open boundaries, and the seabed is represented by high resolution digitised bathymetry. The model was run for a period of one year to determine the spatial distribution of the amplitude and phase of the predominant harmonics, tidal residual currents and their vorticity. Daily variations in the position of amphidromes, as reported by Pugh (1981), are not resolved over this period. The inclusion of more tidal harmonics, updated bathymetric information and long simulation time represent a significant enhancement of modelling fidelity. The aims of this paper are twofold: first, to provide a detailed analysis of tides around the Welsh coast; and second, to provide an integrated source of information on the tidal hydrodynamics of the area. The study area is described in Section 2. In Section 3 a description of the model, its calibration and validation are presented. Section 4 contains the results and discussions of the study and the paper finishes with a short set of conclusions in Section 5.

## 2. Study area description

The study domain covers the Irish Sea and part of the Celtic Sea; having significant areas where the tidal range can be classified as megatidal and is suitable for deployment of tidal range energy devices. Fast flowing currents are of interest for tidal stream energy extraction. The Celtic and Irish Seas are extremely important areas in terms of fish and invertebrate biodiversity, supporting a large diversity of seabirds and marine mammals, along with several important European fisheries [ICES, 2018].

The physical oceanography of the Irish Sea is driven mainly by tidal currents, with tidal streams of 1 m/s in magnitude and water tidal

elevations up to 9 m (Robinson, 1979). Bowden (1980) defined the Irish Sea as comprising an area extending from Carnsore Point (Ireland) and St. David's Head (Wales) in the south to the North Channel between Larne and Corsewall Point to the North. Its width is around 75–140 km and length is approximately 150 km between Ireland and Wales. In its northern area, its largest extent is 195 km from east to west and 150 km from south to north, with the Isle of Man around the centre of the area. The mean volume of the Irish Sea has been estimated as 2430 km<sup>3</sup> and its area as 47,000 km<sup>2</sup> (Howarth, 2005). The run-off fresh water received by the Irish Sea comes from a large catchment area, 43,000 km<sup>2</sup>, mostly arriving from the Eastern Irish Sea (Ribble, Mersey and Dee estuaries; Solway Firth and Morecambe Bay). Also receives a significant contribution of fresh water from the Severn Estuary via the Bristol Channel. According to Howarth (2005) shallow estuaries are found in the area, such as Solway Firth, Morecambe Bay and the Dee Estuary. In addition, extensive sandbanks can be found to the north and east of the Isle of Man (Bahama and King William Banks) and off the Irish coast south of Dublin (Kish, Codling, Arklow and Blackwater Banks). At its southern boundary, St. George's Channel links the Irish Sea with the Celtic Sea. Shallow areas, of depths less than 50 m, can be found to southeast of Cardigan Bay and the east part area of the Isle of Man (Ozer and Legrand, 2015). The Irish Sea is constrained by two narrow channels so waves are predominantly locally generated, with short periods and are often steep. Swell waves in the area are only present near the entrances and southern end of the St. George's Channel. But they also can propagate as far as the Llyn peninsula (North Wales) and the northern part of the Northern Channel (Howarth, 2005).

Cooper (1967) defined the Celtic Sea as a shallow embayment of the eastern North Atlantic Ocean surrounded by the south coast of Ireland, southwest Wales (UK), southwest England (UK) and Brittany (France). According to Pingree (1980), its area can be defined as bordered to the north with the Irish Sea and from the western entrance to the English Channel by a line drawn from Ushant (France) to Land's End (England). The border with the Atlantic Ocean is defined by the 200 m contour water depth (Pingree, 1980). Our high-resolution model grid covers the area shown in Fig. 1.

Tidal ranges at mean spring tides in the area vary between 2 m and around 12 m. Tidal current stresses on the seabed cause the suspension of fine material in the water column occurs due to the movement of sediments and due to the bottom friction of coarser material. The tidal stresses also cause the water column to mix, which can be a significant control on the seasonal thermal stratification in this area (Uncles and Stephens, 2007).

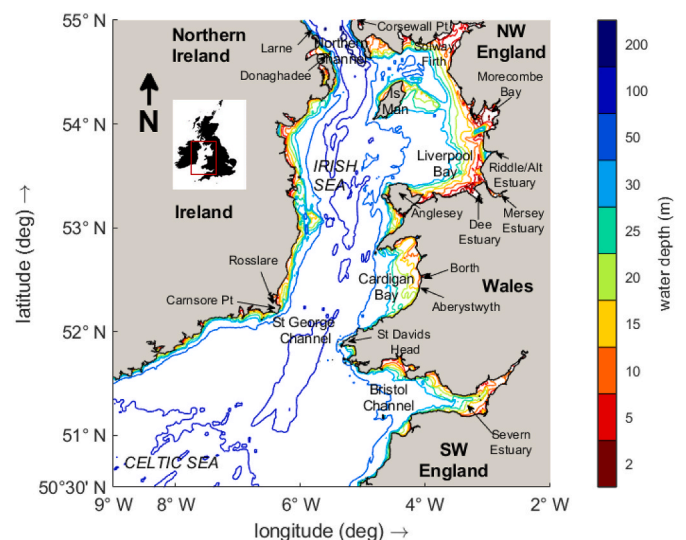


Fig. 1. Location study area (showing bathymetry of the area).

### 3. Computational model

#### 3.1. Delft 3D

In this study, we have employed the hydrodynamic modelling suite Delft3D. Delft3D is an open source three-dimensional (3D) model under active development led by Deltares (<https://oss.deltares.nl/web/delft3d>). It computes solutions to the 3D Navier-Stokes equations using finite-difference approximations with a choice of turbulence schemes and gridding. Here, the model is configured to solve the depth-averaged flow as our primary interest is in the barotropic tidal dynamics. The derivation of the equations used in Delft3D, together with the computational solution method is well documented in the paper by Lesser et al. (2004). The model was configured with nested grids to provide higher resolution for shallow water regions.

#### 3.2. Model domain definition

The hydrodynamic model is based on a set of two structured orthogonal curvilinear spherical grids nested to provide increased resolution in areas where the bathymetry, and flow pattern, is particularly variable. The two domain areas are shown in Fig. 2, in which the Continental Shelf Model (CSM) covers an area which is bounded by latitudes 40°N and 60°N and by longitudes of 20°W and 12°30'E and the Irish and Celtic Seas Model (ICSM) covers the area bounded by latitudes 55°N (Glenarm, NI) and 49°30'N and by longitudes of 5°12'W (Lizard Point, UK) and 10°W. The grid of the CSM model contains 590 × 506 cells and the grid spacing is approximately 3.5 km (0.03°) while the grid of ICSM contains 416 × 304 cells and the grid spacing is less than 2 km (0.0167°). The boundaries of the CSM were chosen to extend beyond the continental shelf, a factor known to be important for modelling the tides

near the coast (Davies and Aldridge 1993). For the ICSM, the grid covers the Welsh coastal waters including the Bristol Channel and estuaries.

The bathymetries for the CSM and the ICSM were taken from ETOPO (Amante and Eakins, 2009), GEBCO 2014 30 arc-second bathymetry (Weatherall et al., 2015) and EMODNET (EMODNET, 2016) and integrated into the model grids converting all levels relative to Mean Sea Level (MSL). A free surface condition was applied to the upper boundary and the bottom boundary was an impermeable bed with a standard formulation of bed shear stress. Specifically, the bed shear stress for the 2D depth averaged flow is induced by a turbulent flow and it is taken to be given by a quadratic friction law as follows, (Lesser et al., 2004):

$$\tau_b = \frac{\rho_0 g \bar{U} |\bar{U}|}{C_{2D}^2}$$

where  $|\bar{U}|$  is the magnitude of the depth-averaged horizontal velocity.

The denominator  $C_{2D}^2$ , is the square of the 2D-Chézy coefficient  $C_{2D}$  [ $\text{m}^{1/2} \text{s}^{-1}$ ].

For the CSM model domain, surface elevations along the open boundaries were obtained from the TPX08.0 OSU Tidal Inversion Software (OTIS - from Oregon State University, <https://www.tpxo.net/global/tpxo8-atlas>) based on Egbert and Erofeeva (2002), by considering 13 tidal constituents: M<sub>2</sub>, S<sub>2</sub>, N<sub>2</sub>, K<sub>2</sub>, K<sub>1</sub>, O<sub>1</sub>, P<sub>1</sub>, Q<sub>1</sub>, MF, MM, M<sub>4</sub>, MS<sub>4</sub> and MN<sub>4</sub>. Surface elevations along the open boundaries for the ICSM model domain are obtained from the CSM model, and interpolated along the boundaries of the nested model. Output was generated after a 5-day spin-up period for both models.

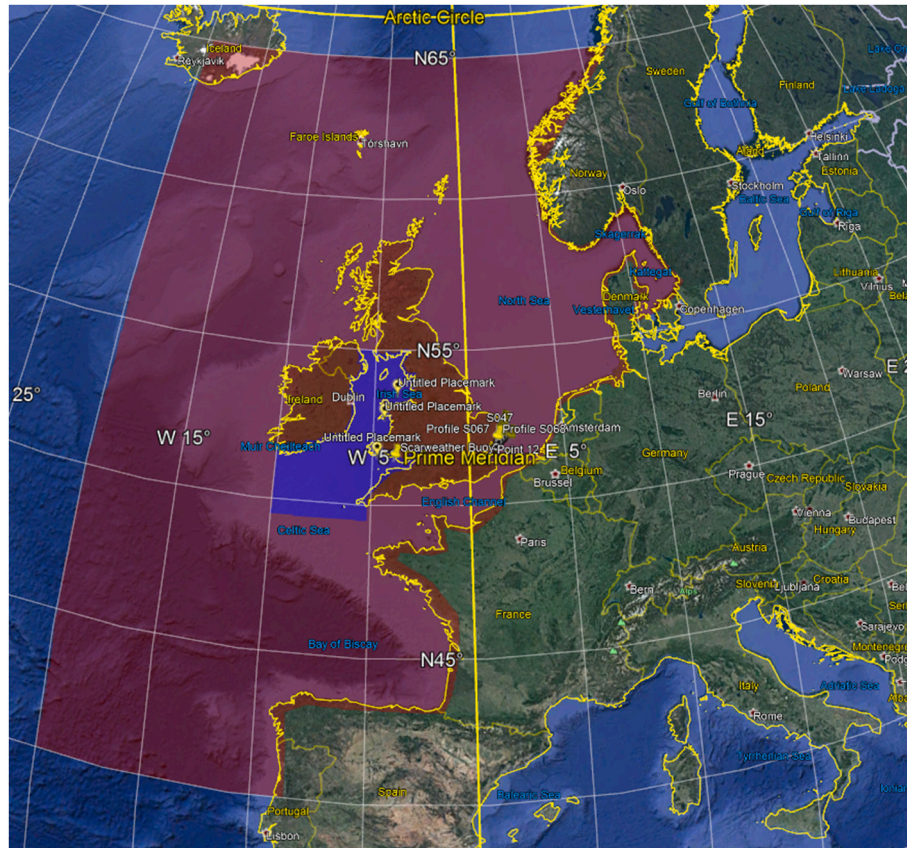


Fig. 2. Limits of the grids used for the tidal models (Continental Shelf Model, CSM – Red; Irish & Celtic Seas Model, ICSM – Blue). Image taken from Google Earth. (For interpretation of the references to colour in this figure legend, the reader is referred to the web version of this article.)

### 3.3. Model calibration

Calibration of the model, specifically to determine the optimum value of the Chézy coefficient, requires comparison of model output against observations. The model generates surface elevations and depth-averaged tidal currents. Observed currents and elevations represent the combined effects of wind, waves and tides. Currents are traditionally measured at one or more discrete depths. To convert these into depth averaged currents against which to compare the results of a depth-averaged model would involve additional assumptions. Here, we focus on surface elevations to avoid such problems and there is no direct test of the instantaneous tidal currents produced by the model.

The computed tidal residual currents are compared against independent observations where the length of record allows surge and storm effects to be smoothed. Comparison of model output against observed surface elevations still has some uncertainties as the model excludes the effects of wind, waves and gradients in sea surface pressure. To mitigate these effects we compare instantaneous surface elevations from the model against observations over a two month period. In addition we compare the amplitude and phase of the dominant tidal harmonics computed from the model output against independent sources.

The calibration of the nested modelling system proceeded in four stages. First, the CSM (coarse grid) model was tested for sensitivity to grid resolution. Computations were performed at three grid resolutions, (5 km, 3.5 km and 1 km), in order to choose the best grid spacing. Computed tidal elevations over the two month period 1st January to March 1, 2003 were compared against measured elevations at all the observation locations shown in Fig. 3. The 3.5 km grid was the best option for these studies giving good results in reasonable computing time. Different time steps (0.25, 0.5, 1.0 and 2.0min) were tested to find an acceptable balance between stability and efficiency. A time step of 2 min was selected. In the second step a set of tests using the 3.5 km grid and 2 min time step were performed for a range of values of the Chézy coefficient. Modelled elevations were again checked against the observations to select the value of Chézy coefficient that gave the least error. The range of values of the Chézy coefficient used for the CSM testing was

40, 55, 60, 65, 75, 90  $m^{1/2}/s$ . Step three involved driving the ICSM with boundary values provided by the calibrated CSM, for grid resolutions of 3.5 km and 1 km and time steps from 0.25 min to 2 min. The optimum values being a resolution of 1 km and a time step of 2 min. The fourth step was to run the ICSM with resolution 1 km and time step 2 min for values of the Chézy coefficient from 60 to 90  $m^{1/2}/s$ .

The calibration results for both models are presented together. Time series of water levels and tidal constituents at the observation points were taken from the tide station toolbox from Delft dashboard (Nederhoff et al., 2016). Measured water levels were recovered from the International Hydrographic Organization, (IHO). Three error metrics were used for the calibration: Root Mean Square Error (RMSE); Correlation coefficient; and percentage RMSE. All quantities were calculated over the results from the two month calibration model runs. Tabulated summaries of calibration statistics for the CSM may be found in Appendix A, Table A1, for the observation points (blue squares in Fig. 3). Tabulated summaries of calibration statistics for the ICSM may be found in Appendix A, Table A2.

Scatter plots for the CSM and ICSM, showing measured elevations versus modelled ones, are presented in Fig. 4 for six stations across the area. The locations are coloured blue in Fig. 3. In each plot, each point represents an hourly value; its x-ordinate being the observed elevation and the y-ordinate being the modelled elevation. The points are colour-coded according to the value of the Chézy coefficient used in the computation. In Fig. 4 the three locations on the left hand side of the figure show a fairly even distribution of points around the perfect fit, ( $y = x$  line). The three locations on the right hand side show a different behaviour. In particular, the spread of points for Hinkley Point is noticeably large, and there is a systematic deviation away from the  $y = x$  line for both Lundy Island and Fishguard. All three of these sites are in the south of the domain and exposed to south-westerly storms, which would contribute a considerable surge components to the measured elevations. Overall, the spread of points is small, indicating a good level of agreement between model and observations.

The values of the Chézy coefficient that provided the best calibrations when considered against all stations shown in Fig. 3 were  $C = 75 m^{1/2}/s$  for the CSM and  $C = 60 m^{1/2}/s$  for the ICSM. A slight change in coefficient between nested grids is not uncommon and reflects the scale-dependent nature of the parameterisation of frictional processes. Overall, the ICSM grid gave improved results in comparison with those from the CSM grid.

### 3.4. Model validation

The process of validation of a model requires testing the calibrated model against a set of observations not used in the calibration procedure. This serves as an independent test of the model, providing additional assurance of its performance. Validation was undertaken over a period of one year, between the February 1, 2015 and the February 1, 2016. This is an extended test but was chosen in order to capture a large range of tidal harmonics. Forty-nine stations were considered in the validation. Modelled elevations at each of the stations for the validation period were subjected to harmonic analysis.

Table 1 shows the RMSE and correlation coefficient between modelled elevations and the IHO data for the CSM and ICSM calculated over the longer validation period of 1 year at the same locations as used for the calibration. When comparing the errors against those in the calibration, (Table A2), it is evident that a very similar level of performance has been achieved against the validation data set.

As a more stringent test of the model than calculating errors between predicted and observed tidal elevations we have chosen to compare the results of an harmonic analysis of the elevations. Table 2 summarises observed and computed amplitudes and phases and their differences for each of the constituents at a selection of stations (Fig. 3). It is noted that some of the largest differences between model and observed phase occur at stations located near amphidromic points. This is not unexpected

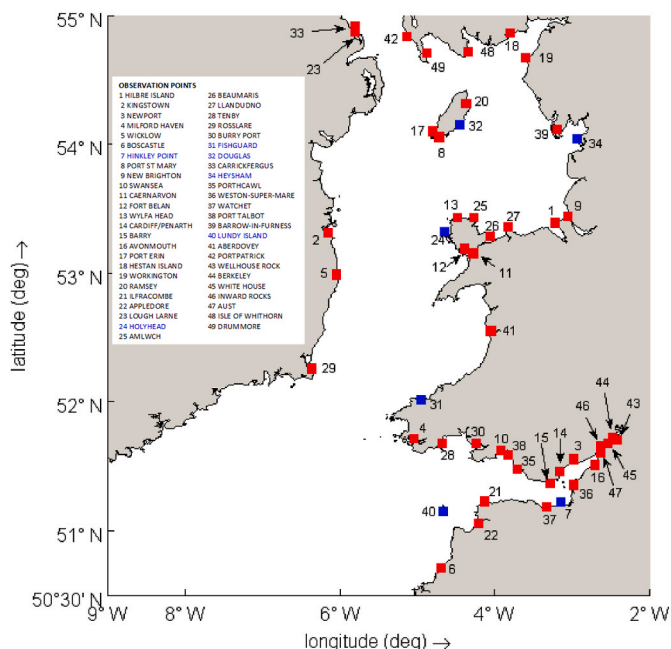


Fig. 3. Locations of observation points used in the calibration and validation process. The observation points that are discussed here appears in blue squares and are denoted in the legend as blue text. Red squares are the points for stringent validation. (For interpretation of the references to colour in this figure legend, the reader is referred to the web version of this article.)

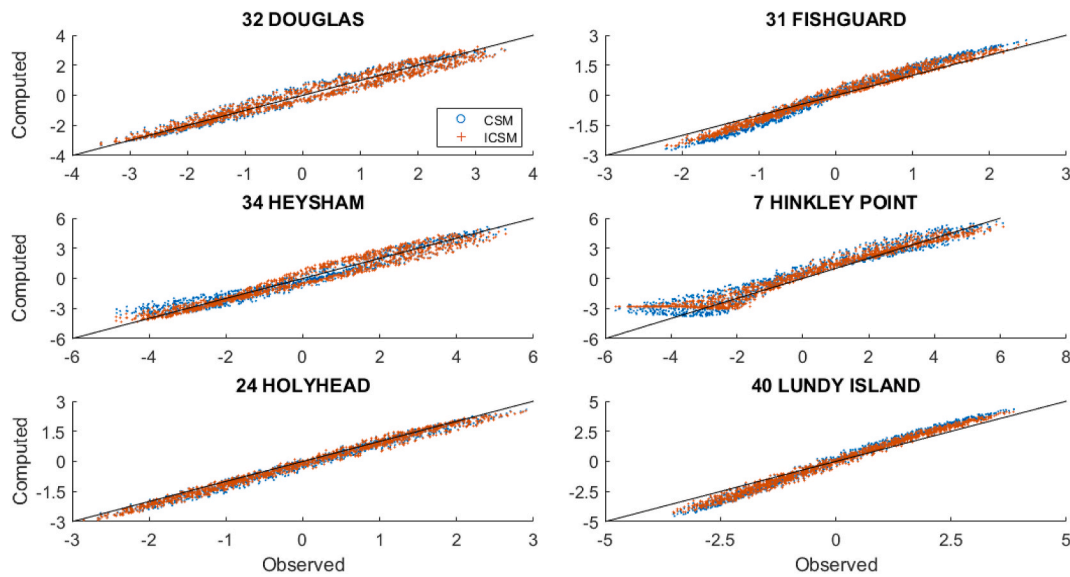


Fig. 4. Scatter plots of modelled and observed surface elevations at six coastal stations for the optimised CSM and ICSM models. Points represent hourly values over the two month calibration period. The CSM and ICSM results are shown in blue and red respectively. (For interpretation of the references to colour in this figure legend, the reader is referred to the web version of this article.)

Table 1  
Validation statistics for a selection of the observation points.

Location	CSM			ICSM		
	RMSE (m)	Correlation Coefficient ( $r^2$ )	Percentage RMSE (%)	RMSE (m)	Correlation Coefficient ( $r^2$ )	Percentage RMSE (%)
32 Douglas	0.401	0.979	6.39	0.408	0.974	5.91
31 Fishguard	0.288	0.993	5.08	0.241	0.992	4.35
34 Heysham	0.555	0.979	5.90	0.566	0.977	5.81
7 Hinkley Point	0.718	0.977	8.54	0.788	0.971	8.36
24 Holyhead	0.189	0.994	3.16	0.180	0.995	3.08
40 Lundy Island	0.462	0.994	5.08	0.431	0.996	4.75

since a small displacement of an amphidromic point can result in dramatic changes in phases. The results in Table 2 were calculated using the harmonic analysis tool within Delft3D.

Table 2 demonstrates that the model reproduced amplitudes and phases along the shoreline to a good level of agreement with IHO data. By inference from continuity considerations it also provides a good estimate of the amplitudes and phases throughout the model domain. Results for the full set of 49 sites are provided in Appendix B. The harmonic amplitudes agree to within 16 cm or better and harmonic phases agree on average to 22° or better across the observation sites.

#### 4. Results and discussions

In this section a detailed description and analysis of tidal properties, including co-tidal charts, tidal asymmetry and tidal current ellipses around the Welsh coastline are presented. All results shown have been computed from the output of the validated ICSM.

##### 4.1. Tidal properties

Based on the classification on tidal range proposed by Davies (1964), and subsequently extended by Levoy et al. (2000), much of the coastline along the Bristol Channel and Morecambe Bay can be classified as mega-tidal (tidal ranges > 8 m), the remainder being macro-tidal (4 m < tidal range < 8 m). In contrast, the tides along the coast of Ireland are meso- or micro-tidal (2 m < tidal range < 4 m and tidal range < 2 m respectively). Our model results confirm that the tidal range along the Welsh coast varies between mega- and macro-tidal. The tidal form factor,  $F$ , (Pugh and Woodworth, 2014), has values less than 0.25

throughout the study area, indicating that the tides in the Irish and Celtic Sea areas are strongly semi-diurnal. Fig. 5 shows the tidal range determined from the CSM. The spatial variation in the amplification of the tidal oscillation around the Celtic/Irish Sea is evident, with macro- and mega-tidal ranges evident around most of the Welsh coast.

##### 4.2. Co-tidal charts

Co-tidal charts show the spatial variation of the amplitude and phase of an individual tidal harmonic, illustrating the relative contribution of that harmonic to the total tidal flow. Co-tidal charts, calculated from the ICSM tidal elevation output, for the main tidal harmonics  $O_1$ ,  $K_1$ ,  $N_2$ ,  $M_2$  and  $S_2$  are shown in Fig. 6. These are in good qualitative agreement with earlier results derived from point observations by Mungall and Matthews (1978), Robinson (1979) and Howarth (1990).

The charts in Fig. 8 also compare well in general terms with those obtained with coarser grid circulation models, such as Davies and Jones (1992), while providing additional detail.

Furthermore, the position of the amphidromic point of the  $M_2$  harmonic near the Irish coast agrees well with the position suggested by the analysis of tide gauge observations presented by Robinson (1979) and Howarth (1990). The amplitudes in Fig. 6 clearly demonstrate that semi-diurnal tides are the significant constituents in this study area, and that the  $M_2$  harmonic is the predominant harmonic.

One important feature of the two major semi-diurnal tides ( $M_2$  and  $S_2$ , Fig. 8) is that their amplitudes increase remarkably along the Welsh and English coasts but are damped along the Irish coast when they propagate into the Irish Sea. This can in part be explained by the Coriolis effect that acts to divert the tidal wave propagation path towards the

**Table 2**  
Amplitude, A (in metres), and phase, ph (in degrees), from a selection of the IHO tidal stations included in Delft Dashboard (Nederhoff et al., 2016), model results and their differences.

	O <sub>1</sub>		K <sub>1</sub>		N <sub>2</sub>		M <sub>2</sub>		S <sub>2</sub>		M <sub>4</sub>		MS <sub>4</sub>		M <sub>6</sub>	
	A	ph	A	ph	A	ph										
<b>6 BOSCASTLE</b>																
Measured	0.050	17.1	0.060	113.0	0.460	104.6	2.360	143.0	0.890	201.0	0.130	32.0	0.160	65.0	-	-
Model	0.057	354.1	0.048	110.4	0.523	138.3	2.737	158.6	0.955	202.5	0.056	181.0	0.053	238.4	0.013	252.8
Difference	0.007	-23.0	-0.012	-2.6	0.063	33.7	0.377	15.6	0.065	1.5	-0.074	149.0	-0.107	173.4	-	-
<b>7 HINKLEY POINT</b>																
Measured	0.100	330.0	0.070	105.0	0.780	165.0	3.800	185.0	1.420	237.0	0.120	2.0	0.050	351.0	0.040	222.0
Model	0.055	29.1	0.046	154.5	0.504	202.0	3.199	219.8	0.909	271.5	0.232	356.7	0.214	62.4	0.101	130.1
Difference	-0.045	59.1	-0.024	49.5	-0.276	37.0	-0.601	34.8	-0.511	34.5	0.112	-5.3	0.164	71.4	0.061	-91.9
<b>24 HOLYHEAD</b>																
Measured	0.094	34.4	0.107	181.3	0.360	267.3	1.788	291.8	0.591	328.3	0.029	38.7	0.009	105.4	0.023	216.9
Model	0.085	42.5	0.060	173.0	0.354	264.2	1.789	289.5	0.607	327.2	0.046	349.9	0.030	43.7	0.014	251.1
Difference	-0.009	8.1	-0.047	-8.3	-0.006	-3.1	0.001	-2.3	0.016	-1.1	0.017	-48.8	0.021	-61.7	-0.009	34.2
<b>29 ROSSLARE</b>																
Measured	0.073	44.3	0.065	182.6	0.102	140.6	0.562	159.5	0.252	220.9	0.035	51.3	0.012	91.4	0.005	320.4
Model	0.059	49.2	0.035	161.8	0.169	176.3	0.875	186.3	0.355	242.9	0.048	207.7	0.035	269.6	0.019	0.5
Difference	-0.014	4.9	-0.030	-20.8	0.067	35.7	0.313	26.8	0.103	22.0	0.013	156.4	0.023	178.2	0.014	40.1
<b>31 FISHGUARD</b>																
Measured	0.073	4.0	0.085	158.0	0.299	186.0	1.317	207.0	0.524	247.0	0.104	16.0	0.055	62.0	-	-
Model	0.068	21.8	0.050	142.2	0.347	190.0	1.730	210.1	0.652	253.4	0.024	155.0	0.017	280.2	0.007	90.9
Difference	-0.005	17.8	-0.035	-15.8	0.048	4.0	0.413	3.1	0.128	6.4	-0.080	139.0	-0.038	-141.8	-	-
<b>32 DOUGLAS</b>																
Measured	0.159	38.0	0.098	181.0	0.472	301.0	2.274	326.0	0.756	9.0	0.049	226.0	0.055	232.0	-	-
Model	0.089	60.2	0.063	195.2	0.393	310.5	2.096	336.5	0.647	18.2	0.044	52.1	0.029	119.9	0.022	9.9
Difference	-0.070	22.2	-0.035	14.2	-0.079	9.5	-0.178	10.5	-0.109	9.2	-0.005	-173.9	-0.026	-112.1	-	-
<b>33 CARRICKFERGUS</b>																
Measured	0.073	32.0	-	-	0.219	295.0	1.143	317.0	0.320	352.0	0.003	277.0	0.009	175.0	-	-
Model	0.077	49.1	0.049	190.9	0.119	282.3	0.582	319.1	0.110	349.2	0.024	256.6	0.010	328.9	0.017	196.8
Difference	0.004	17.1	-	-	-0.100	-12.7	-0.561	2.1	-0.210	-2.8	0.021	-20.4	0.001	153.9	-	-
<b>34 HEYSHAM</b>																
Measured	0.104	3.0	0.116	185.0	0.619	310.0	3.274	328.0	1.155	6.0	0.128	265.0	0.122	298.0	-	-
Model	0.097	66.6	0.075	203.4	0.533	330.2	2.994	349.9	0.920	40.5	0.366	276.1	0.270	325.2	0.035	157.1
Difference	-0.007	63.6	-0.041	18.4	-0.086	20.2	-0.280	21.9	-0.235	34.5	0.238	11.1	0.148	27.2	-	-
<b>40 LUNDY ISLAND</b>																
Measured	0.050	350.0	0.080	122.0	0.470	144.0	2.340	164.0	0.820	209.0	0.060	314.0	0.030	7.0	0.030	143.0
Model	0.058	358.5	0.048	115.0	0.546	149.6	2.860	169.9	1.003	214.6	0.056	241.2	0.055	296.0	0.010	303.7
Difference	0.008	8.5	-0.032	-7.0	0.076	5.6	0.520	5.9	0.183	5.6	-0.004	-72.8	0.025	-71.0	-0.020	160.7
<b>42 PORTPATRICK</b>																
Measured	0.100	42.0	0.110	190.0	0.260	306.0	1.340	333.0	0.380	16.0	0.010	277.0	0.010	107.0	-	-
Model	0.081	56.6	0.056	196.0	0.192	307.8	1.005	340.4	0.262	21.0	0.012	236.0	0.004	241.9	0.012	176.2
Difference	-0.019	14.6	-0.054	6.0	-0.068	1.8	-0.335	7.4	-0.118	5.0	0.002	-41.0	-0.006	134.9	-	-
<b>48 CASTLETOWNSHEND</b>																
Measured	0.020	309.0	0.020	57.0	0.220	109.0	1.090	133.0	0.340	164.0	0.040	263.0	0.020	344.0	-	-
Model	0.016	39.5	0.022	68.5	0.225	125.8	1.152	149.6	0.346	186.9	0.032	31.8	0.024	108.0	0.012	150.2
Difference	-0.004	90.5	0.002	11.5	0.005	16.8	0.062	16.6	0.006	22.9	-0.008	128.8	0.004	124.0	-	-
Average	0.020	24.0	0.039	34.3	0.090	14.4	0.356	12.8	0.179	13.5	0.055	74.3	0.050	105.8	0.026	81.7
RMSE	0.029	31.6	0.040	60.0	0.114	19.3	0.400	17.1	0.223	18.4	0.092	96.6	0.076	115.9	0.025	72.7

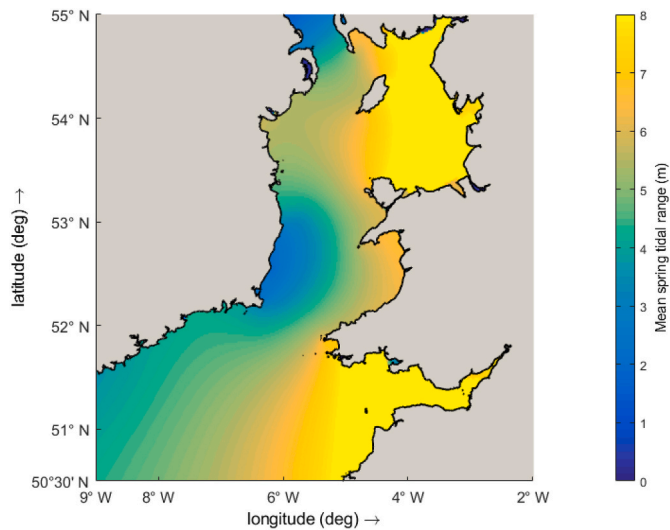


Fig. 5. Tidal range in the Celtic/Irish Sea from the CSM.

right, but in the main by the resonance properties of this sea region. Specifically, an approximate calculation tells us that as the distance from Fishguard (St. George's Channel) to Stranraer (southern end of North Channel) is roughly 300 km and the mean depth of the sea between the two is close to 100 m the propagation speed of a long wave will be approximately 30 m/s. So if the tidal period is 12 h, a quarter wavelength region will have a length of about 300 km. The dimensions of the Irish Sea are almost perfect for creating a resonant response. This may explain in part the relative insensitivity of our results to small changes in Chézy coefficient, where other authors have found resonance phenomena to be sensitive to the choice of this parameter, (e.g. Gao and Adcock, 2017). In reality, the Irish Sea is not rectangular but of irregular shape, its bathymetry is not constant but varies considerably, and the progression of the tide wave is affected by Coriolis accelerations. In the North Sea the Coriolis effect causes the tidal wave to propagate in an anticlockwise sense around the shoreline, with largest amplitudes at the coast and an amphidrome towards the middle of the North Sea, (Howarth 1990). In contrast, the Irish Sea is not sufficiently broad to allow the tide wave to propagate around its edges without interference. Taylor (1919) found that the tidal movement within the Irish/Celtic Sea was a co-oscillating response of the shelf sea to the tides generated in the Atlantic Ocean. Taking the  $M_2$  constituent as an example, its amplitude is about 3.6 m in the middle of the Severn Estuary (England and Wales) and decreases to less than 0.5 m in the Irish Coast (Rosslare area) and increase again towards the Liverpool Bay area to 3.0–3.3 m. Two amphidromic points ( $M_2$  component) can be found in this area: one in the North Channel (not shown), and one “degenerate” amphidromic point (where cotidal lines join on a point inland), in St. George's Channel. The other main semi-diurnal harmonics,  $N_2$  and  $S_2$ , show a pattern similar to that of  $M_2$  but with diminished magnitude. The diurnal harmonics,  $O_1$  and  $K_1$ , show a different pattern from the semi-diurnal harmonics as might be anticipated from their larger wavelength and period. The co-tidal charts (Fig. 8a,b,c) show a rapid increase in amplitude and phase from the Celtic Sea into the Irish Sea, with a maximum amplitude in the Severn Estuary and Liverpool Bay.

According to Huntley (1980), in the Irish Sea the tide moves with a “rocking” motion where the occurrence of the high waters is alternates at the open and closed ends of the sea with a small tidal range in the central region. This behaviour is evident in the approximate  $180^\circ$  phase difference in both  $M_2$  and  $S_2$  constituents between the northern and southern parts of the domain. That is, at the time of high water in the northern end of the Irish Sea, it is low water in the southern end. It suggests too, the existence of strong tidal streams in the central part of this region that is characteristic of standing-wave motion.

Fig. 7 shows the co-tidal charts of the main shallow water harmonics ( $MS_4$ ,  $MN_4$ ,  $M_6$ ,  $M_4$ ,  $2SM_6$ ,  $2MS_6$ ,  $2MN_6$ ) determined from the ICSM, giving an integrated picture of these harmonics for the entire Welsh coastal waters. Our results for  $M_4$  and  $M_6$  show good general agreement with those of Davies (1986) who used a relatively coarse resolution three dimensional finite difference model of the Northwest European continental shelf to simulate the  $M_4$  harmonic, and also with the results of Jones and Davies (1996) who presented results for  $M_4$  and  $M_6$ . The higher grid resolution of our model reveals additional fine structure. It is also clear from Fig. 7 that in estuarine regions, such as Morecombe Bay, Solway Firth in Liverpool Bay and in the Severn Estuary, there are rapid changes in the amplitude of shallow water harmonics over small distances.

Of the shallow water harmonics,  $M_4$  is the dominant one, followed by  $MS_4$ ,  $MN_4$ ,  $2MS_6$ ,  $M_6$  and  $2SM_6$  (Fig. 7). According to Andersen (1999) the  $M_4$  tidal harmonic is the largest shallow water constituent in the northwest European Shelf region. This is confirmed at a regional level by our results that show  $M_4$  has a mean amplitude of approximately 4.3 cm over the domain with values  $> 15$  times larger at some locations such as the Severn Estuary, the Mersey Estuary and Morecombe Bay. However, there are localised exceptions to this general picture where, for example,  $MS_4$  is of comparable or greater magnitude. The three harmonics  $M_4$ ,  $MS_4$  and  $MN_4$  all exhibit an amphidromic point to the northeast of the Isle of Man.

The harmonic  $MS_4$  has a similar pattern to  $M_4$  but with smaller amplitudes.  $MS_4$  has a mean amplitude of approximately 3.7 cm over the domain with maximum values  $> 13$  times larger at several locations in the Severn Estuary and an amphidromic point in Cardigan Bay. The harmonic  $MN_4$  shows a similar pattern to those of  $M_4$  and  $MS_4$ . The  $MN_4$  harmonic has average amplitude of 1.5 cm with amplitudes beyond 20 cm at the Dee Estuary and Severn Estuary.

The last of the more dominant harmonics considered here is  $2MS_6$ . This harmonic has a mean amplitude of 1.6 cm, with amplitudes exceeding 15 cm in the Severn Estuary and the Dee Estuary. The most significant shallow water harmonics in this region are  $M_4$ ,  $MS_4$ ,  $MN_4$  (quarter-diurnal constituents) and  $M_6$ ,  $2SM_6$ ,  $2MS_6$ ,  $2MN_6$  (sixth diurnal). Shallow water harmonics arising from interactions with diurnal harmonics  $K_1$  and  $O_1$  tend to be weak.

#### 4.3. Tidal asymmetry

Friedrichs and Aubrey (1988) describe two measures of tidal asymmetry. The first is the total distortion factor, which is defined as the ratio of the amplitudes of  $M_4$  and  $M_2$ :  $A_{M_4}/A_{M_2}$ . If  $A_{M_4}/A_{M_2} > 0.01$ , significant distortion of the tidal wave is expected. The second is the tidal dominance factor which is defined in terms of the phases of the harmonics  $M_2$  and  $M_4$ :  $|2\phi_{M_2} - \phi_{M_4}|$ . If  $|2\phi_{M_2} - \phi_{M_4}|$  is between  $0^\circ$  and  $180^\circ$ , the tide is flood dominant and if it is between  $180^\circ$  and  $360^\circ$ , the tide is ebb dominant. The relevance of these to tidal energy generation and net transport of sediments may be viewed as follows. Tidal energy exploitation is concentrated on shallow continental shelves, exactly where shallow water harmonics may be largest. The presence of shallow water harmonics will produce asymmetries in the tidal oscillation and consequently power extraction, reducing the overall energy yield, (Neill et al., 2012). Similarly, asymmetries in the flood and ebb flows will lead to inequalities in the durations for which near bed currents exceed the threshold velocity and hence differences between the quantity, direction and distance of sediment transport on the ebb and flood tides, leading to a net drift, Prandle (2009).

Fig. 8 shows the parameters for tidal distortion and asymmetry in the Irish and Celtic Seas. Fig. 8a shows that the areas where the tide is less distorted, ( $A_{M_4}/A_{M_2} < 0.01$ ), are mostly outside the estuaries. The greatest tidal distortions are found in the estuaries (e.g., Severn, Dee, Mersey, Ribble and Alt, Solway Firth, Milford Haven, etc.). Also highly distorted tides are present along a section of the open Irish coast (from

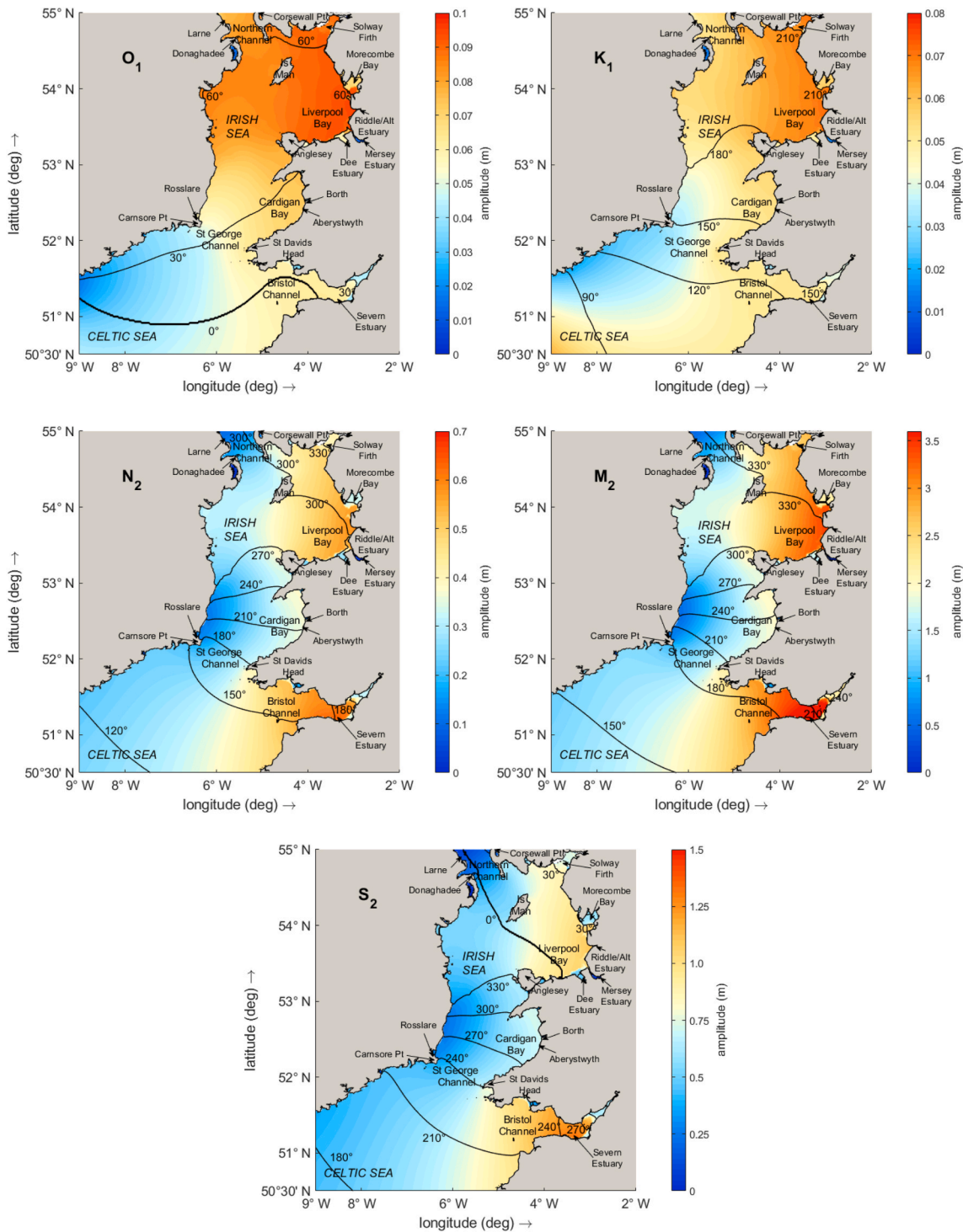


**Fig. 6.** Co-tidal charts for the main constituents ( $O_1$ ,  $K_1$ ,  $N_2$ ,  $M_2$ ,  $S_2$ ) calculated over one-year period (1st February 2015 – 1st February 2016). The colour bar represents the amplitudes and the black solid lines represent the phases of the constituents. Note that the amplitude range changes in each panel while the colour range remains the same. (For interpretation of the references to colour in this figure legend, the reader is referred to the web version of this article.)

Rosslare up to Donaghadee, Northern Ireland). High tidal distortion coincides with the areas of high  $M_4$  amplitude (Fig. 6, co-tidal chart  $M_4$  and  $M_2$ ), as might be expected. The tidal dominance factor is shown in Fig. 8b. The Severn Estuary and the estuaries around Liverpool Bay are flood dominant. Within Cardigan Bay the north part of the bay is flood-dominant and the middle and south parts are ebb-dominant. A similar pattern in the tidal dynamics occurs along the Irish coast, (between Rosslare and Wicklow), where a transition of tidal dominance is present. The same happens in the Northern Channel between Lough Larne and

Port Patrick (stations 23 and 42 in Fig. 3). The transitions correspond to the nodal lines of a standing wave oscillation described in Section 4.2, which explains the large tidal range experienced along the Liverpool Bay coastal area.

From a dynamical perspective, a large distortion factor indicates frictional energy dissipation arising in shallow waters and transfer of energy from  $M_2$  to  $M_4$ , through nonlinear processes, (Aubrey and Speer, 1985; Friedrichs and Aubrey, 1988). The distortion of the tidal oscillation in estuaries may be understood from this perspective. However, off

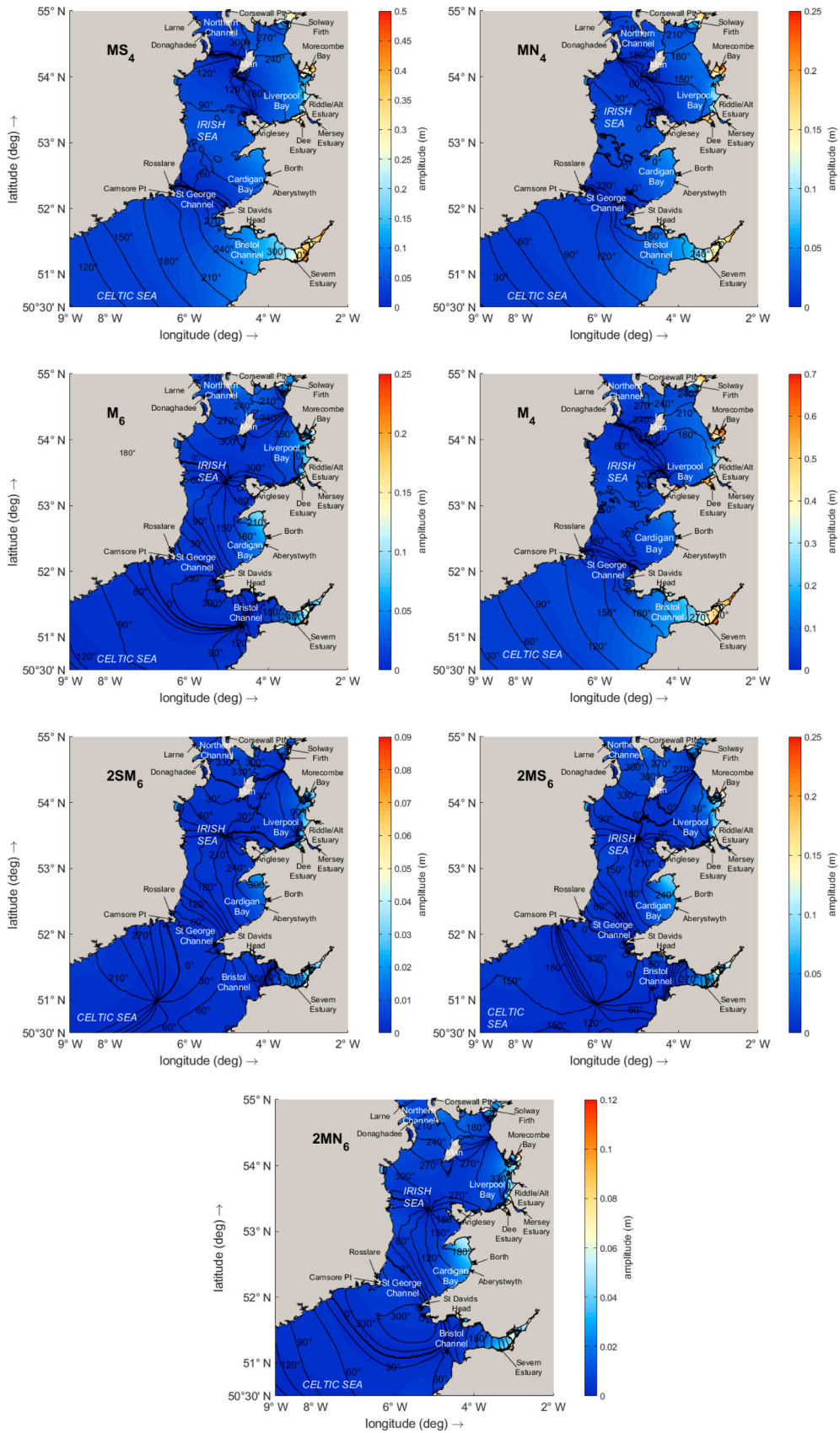


**Fig. 7.** Co-tidal charts for the shallow water constituents (MS<sub>4</sub>, MN<sub>4</sub>, M<sub>6</sub>, M<sub>4</sub>, 2SM<sub>6</sub>, 2MS<sub>6</sub>, 2MN<sub>6</sub>). The colour bar represents the amplitudes and the black solid lines represent the phases of the constituents. (For interpretation of the references to colour in this figure legend, the reader is referred to the web version of this article.)

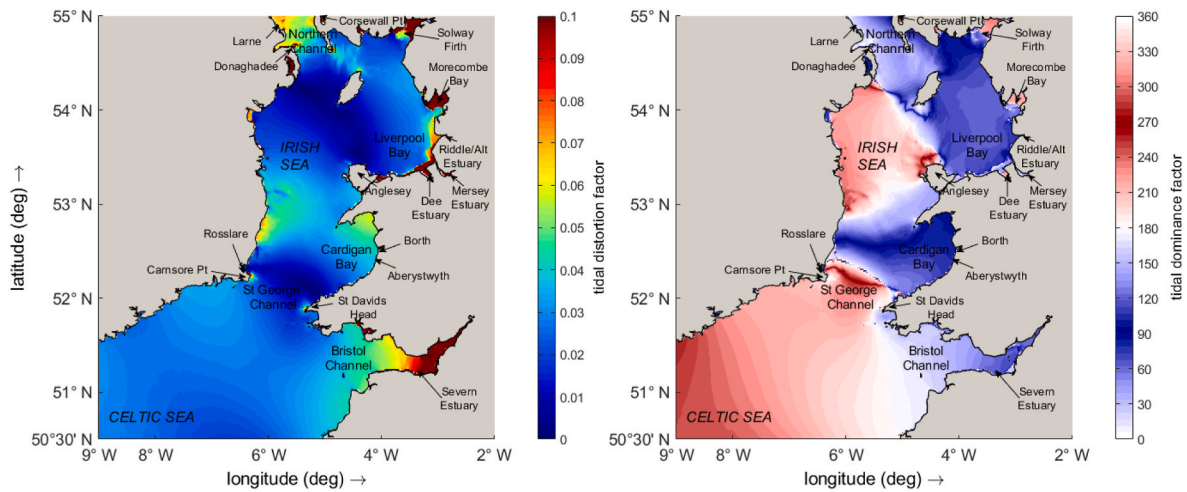


Fig. 8. a) Tidal distortion ( $AM_4/AM_2$ ) indicator and b) tidal dominance ( $2\phi_{M_2} - \phi_{M_4}$ ) indicators (criteria from Friedrichs and Aubrey, 1988).

the east coast of Ireland, in the vicinity of an amphidrome of  $M_2$ , the resulting diminished amplitude of  $M_2$  allows greater prominence to  $M_4$  and consequent tidal distortion.

#### 4.4. Tidal ellipses

The contribution of each tidal harmonic to the depth-averaged tidal flow may be found using harmonic analysis, applied to each component of the horizontal velocity. The constants from each component of velocity may be combined to construct an ellipse that describes the tidal motion due to an individual tidal harmonic, (Howarth 1990). Tidal ellipses encapsulate information about the maximum and minimum tidal current speeds and directions, the sense of rotation of the tidal current, and the flow in relation to the state of the tide. A long thin ellipse indicates almost rectilinear tidal flow, with a rapid switch between flood and ebb flows. In contrast, broad, almost circular ellipses indicate the tidal current speed is almost constant as the direction changes. The sense of rotation is affected by the geometry of the seabed, the shape of the coastline and the Coriolis effect. The latter will tend to create clockwise rotation (in the Northern hemisphere).

Time histories of the tidal currents computed in the ICSM over the one-year validation period were analysed to extract the harmonic constants. The tidal ellipse parameters for the  $M_2$  tidal constituent at each grid point were calculated from the corresponding time histories. The results are shown in Figs. 9 and 10 (a-e) with red and blue denoting clockwise and anti-clockwise rotation respectively. Fig. 9 shows the general distribution of the tidal ellipses every ten grid points for the ICSM area, while Fig. 10 shows results for enlarged subregions.

Tidal ellipses are aligned along channel axes in: St George’s Channel; the Bristol Channel; and the Northern Channel, indicating that rotation is relatively unimportant due to the geometrical constraints. The ellipses are very elongated, typically with their minor axis being less than 10% of their major axis. Broader tidal ellipses occur at the intersection of channels, due to transverse reflection effects, and in Morecombe and Cardigan Bays where the localised broadening of channels creates a more relaxed tidal flow. The general trend of the tidal ellipses for the  $M_2$  constituent is similar to the tidal current circulation patterns presented in the previous section, and also reflects the change in tidal phase or ‘rocking’ pattern associated with the standing wave nodal lines discussed in Section 4.2.

Tidal ellipses close to the shore and to the north of Anglesey, Llyn Peninsula and Pembrokeshire have their major axis aligned with the coast and are highly elongated. Immediately to the south the tidal ellipses become more rounded, where there is no slack water. Both Anglesey and Pembrokeshire lie close to regions which switch from

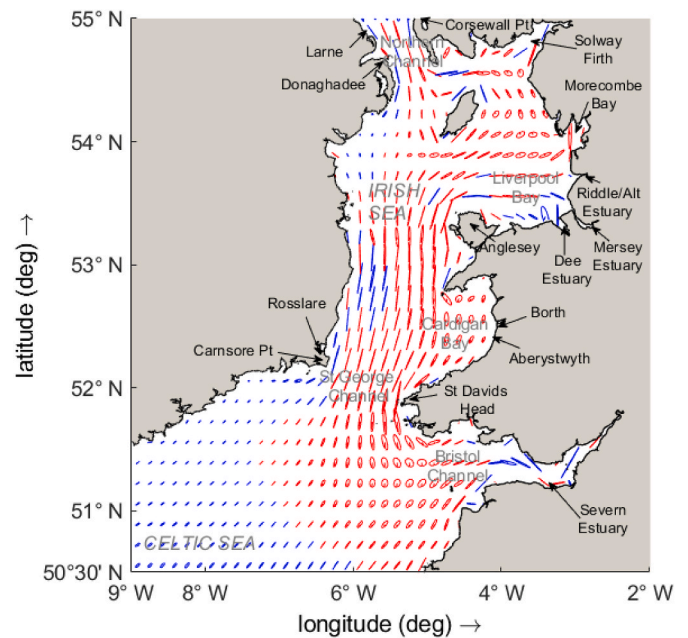
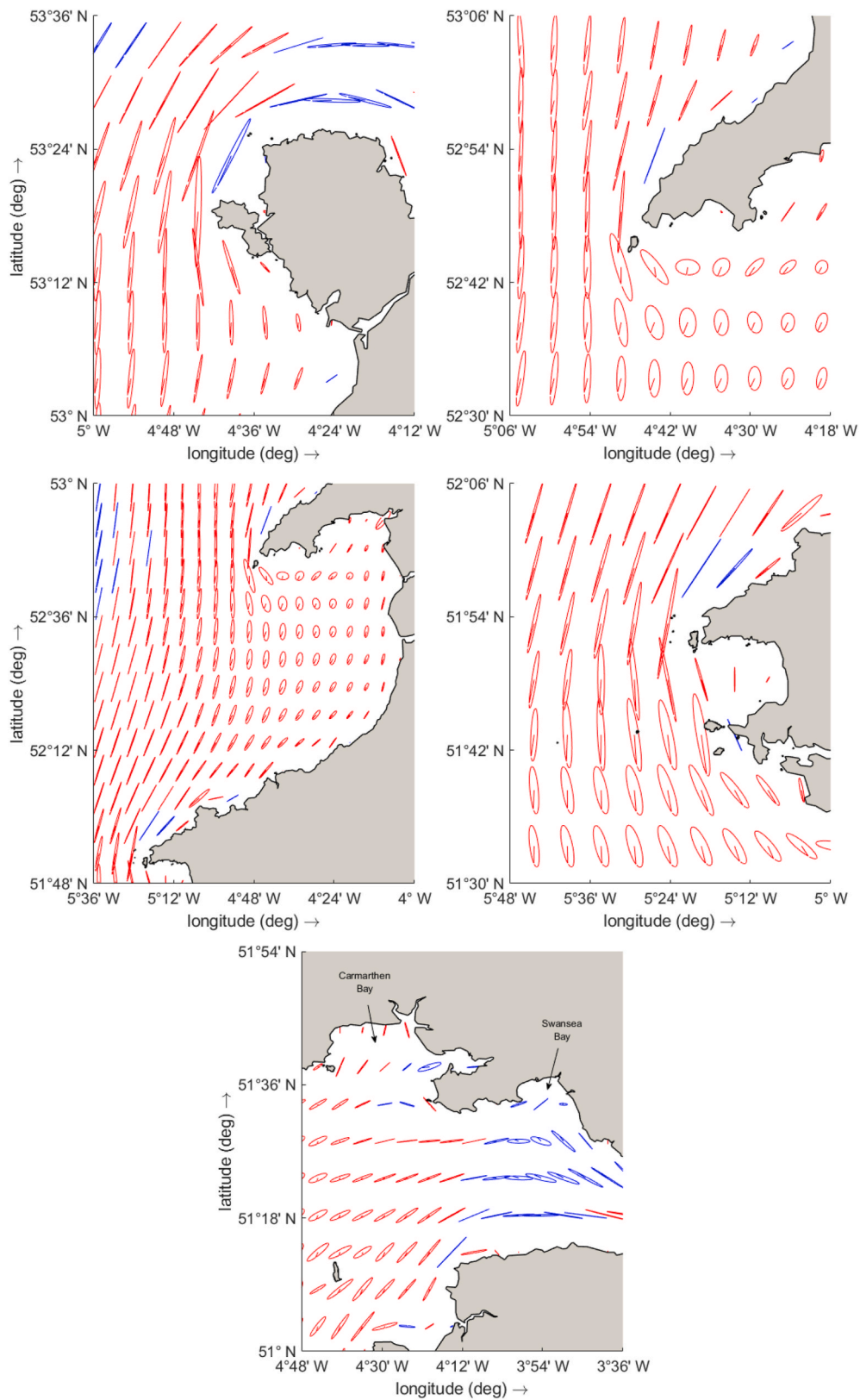


Fig. 9. Tidal current ellipses of the  $M_2$  tide constituent calculated every ten grid points from the depth-averaged tidal velocities over one year. Clockwise (blue), anticlockwise (red). (For interpretation of the references to colour in this figure legend, the reader is referred to the web version of this article.)

being ebb dominated to the north to flood dominated to the south, while the Llyn Peninsula is something of an exception as it experiences flood dominant tides to north and south. It is possible to find major to minor ellipse axis ratios of around 0.4 near Ramsey Island (Pembrokeshire, Figs. 10c) and 0.2 - 0.3 near Anglesey and Llyn Peninsula (Fig. 10a and b).

Fig. 10a shows that to the north of Anglesey, the ellipses indicate clockwise rotation of the tide; to the northwest there is a combination of clockwise and anticlockwise rotation and towards the west of Anglesey the tidal ellipses are more rectilinear and elongated and have anti-clockwise rotation. Near to the Llyn Peninsula (Fig. 10b), the tidal ellipses show anticlockwise tidal rotation and are elongated; towards the west of the peninsula and to the south, the tidal ellipses show anti-clockwise tidal rotation but have a tendency to be less elongated and more circular. Inside Cardigan Bay (Fig. 10c), most of the tidal ellipses show anticlockwise tidal rotation and are more circular than in the other



**Fig. 10.** Tidal current ellipses of the M2 tide constituent calculated every ten grid points from the depth-averaged tidal velocities over one year. For a) Anglesey, b) Llyn Peninsula, c) Cardigan Bay, d) Pembrokeshire and e) Carmarthen and Swansea Bays. Clockwise (blue), anticlockwise (red). (For interpretation of the references to colour in this figure legend, the reader is referred to the web version of this article.)

areas. Moving westwards out of the Bay, the tidal ellipses become more elongated than inside the bay, indicating transition to more rectilinear flow.

#### 4.5. Tidal residuals

##### 4.5.1. Residual currents

Residual tidal currents were calculated as grid point averages of instantaneous currents at each time step over the year-long validation run of the ICSM. The residual currents show a complex flow pattern, with several gyres in the area of the Eastern Irish Sea Basin, Cardigan Bay and the Welsh coast in the Severn Estuary. Plots of residual currents for selected areas are shown in Fig. 12 in the following section.

The residual currents are relatively weak, (<0.1 m/s), and around 0.01 m/s in most places. The general sense of the flow is from the Atlantic in the direction from south to north near the coasts with a more complicated pattern around St George’s Channel. Part of the main flow diverts towards the Welsh coast moving northwards approaching the Isle of Man. One part enters the eastern Irish Sea (North of Anglesey) and gyres anti-clockwise near the Isle of Man rejoining the main flow northward to North Channel. In the middle of the Eastern Irish Sea an anti-clockwise gyre is apparent, which was also noted by Ramster and Hill (1969) in their study of the tidal circulation of the Northern Irish Sea using Woodhead seabed drifter and current meter measurements. Anti-clockwise gyres are also evident in Liverpool Bay and the outer Bristol Channel near Ilfracombe.

The magnitudes of the computed tidal residual currents are in good qualitative agreement with the study of Ramster and Hill (1969) for the Northern Irish Sea, and are in agreement with the patterns obtained by other studies such as the observational campaign of Robinson (1979) and the national scale studies of Brown et al. (2015) and Williams et al. (2019). The southward residual flow to the north of Anglesey is at variance to the results found by Prandle and Ryder (1989) who compared surface currents derived from radar measurements with depth-averaged currents from a computational model. They found reasonable agreement between the two for the M<sub>2</sub> harmonic but less so for the M<sub>4</sub> harmonic. The radar measurements indicated a northward residual current leading to unrealistic estimates of flow. The residual currents computed from our depth-averaged model are smaller and reflect the seabed geometry as they are unable to distinguish flow variations with depth.

##### 4.5.2. Vorticity

The strength of the circulatory flow in residual current patterns may be measured conveniently by its vorticity. For horizontal flows, such as the residual currents of the depth-averaged flow, the vertical component of the vorticity,  $\xi$ , is the only non-zero component and may be written as:

$$\xi = \frac{\partial V}{\partial x} - \frac{\partial U}{\partial y} \quad (3)$$

where the depth integrated residual current is ( $U, V$ ) and  $x$  and  $y$  are local Cartesian coordinates running in west to east and south to north directions respectively. It follows from this definition that positive and negative vorticity correspond to anticlockwise (cyclonic) and clockwise (anticyclonic) circulations respectively. Prandle and Ryder (1989) presented measurements of coastal vorticity together with linkages between depth-averaged equations and vorticity. They concluded that the magnitude of the vorticity was of the same order as the accuracy of their calculations. Subsequent advances in modelling technology and computing power have led to the improvement of the accuracy of results. Calculation of the vorticity of tidal residuals has been presented, for example, by Neill (2009) and Yang and Wang (2013) to investigate sediment transport and water exchange in coastal waters. As noted in the Introduction, the analysis of residual currents and their vorticity is best viewed as a diagnostic tool for interpreting potential sediment transport

trends, pollutant and water movements. The vorticity at each point of the grid was calculated using a centred finite difference scheme coded in MATLAB®, and included the additional metric terms associated with the spherical coordinate system used in Delft3D.

Fig. 11 shows colour-flooded contour plot of the vorticity of the residual currents over the whole domain and Fig. 12 shows enlarged plots for Anglesey, Llyn Peninsula, Cardigan Bay and Pembrokeshire with the residual currents superimposed. Vorticity extrema in the residual flow are found in areas where sandbanks, headlands and abrupt changes to bathymetry are located. Residual flows in the Severn Estuary and estuaries around Liverpool Bay have large vorticity. In the Severn the pattern of predominantly positive vorticity along the English coast and negative vorticity along the South Wales coast is indicative of upstream flow along the edges of the estuary and downstream flow along the centre of the channel. There are also areas where the vorticity of the residual flow is close to zero, such as in Cardigan Bay away from the coastline and off the Irish coast between Rosslare and Donaghadee. Linear patches of positive/negative vorticity emanating from the south coast of Ireland into the Irish Sea coincide with sandbanks with similar dimensions. Typical values of the magnitude of vorticity are of the order of  $10^{-5}$  to  $10^{-6} \text{ s}^{-1}$ , which corresponds to the value found in other studies around the North Sea and the continental shelf, such as Nihoul and Ronday (1975); Zimmerman (1978), Zimmerman (1981) and Horrillo-Caraballo and Reeve (2008).

Fig. 12a shows a large area of positive vorticity towards the western part Anglesey which corresponds to a major gyre in the residual current. This is attributable in large part to the amplification in the north-westerly residual flow while approaching the Anglesey coastline, rather than the formation of a strong circulatory flow. Shoreward of this gyre (northwest part of the Isle) is a region of negative vorticity. There are also many smaller residual eddies. On the northeast coastline of Anglesey, the vorticity is positive and to the northwest tends to be negative. An elliptical anticlockwise residual gyre is located on the west side of Anglesey.

Areas of positive and negative vorticity are apparent in Fig. 12b southwest of the tip of the Llyn Peninsula, west of Bardsey Island. A gyre with positive vorticity is clearly visible while the area of negative vorticity to its northwest also corresponds to a gyre which is slightly weaker. The formation of such a ‘dipole’ is readily understood from the arguments proposed by Pingree (1978), Zimmerman (1978) and Robinson (1983) who argued that flood and ebb flows would set up transitory eddies on the lee side of a promontory which, when averaged over one or more tidal cycles would yield a dipole pattern.

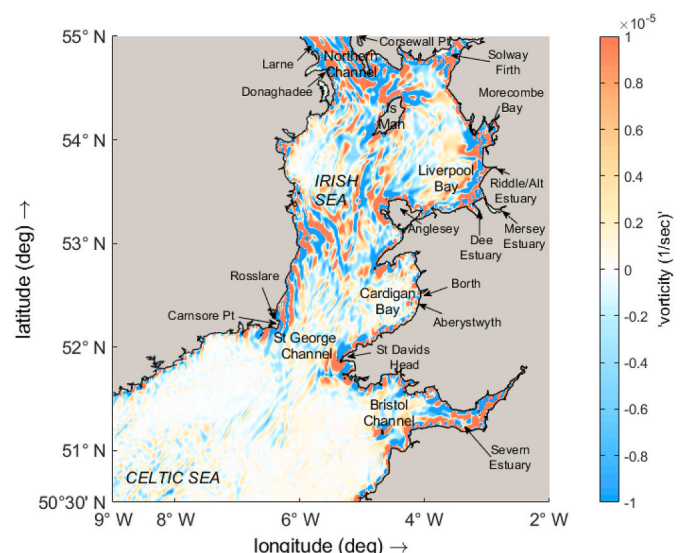


Fig. 11. Vorticity field of the residual currents in the Celtic and Irish Seas.

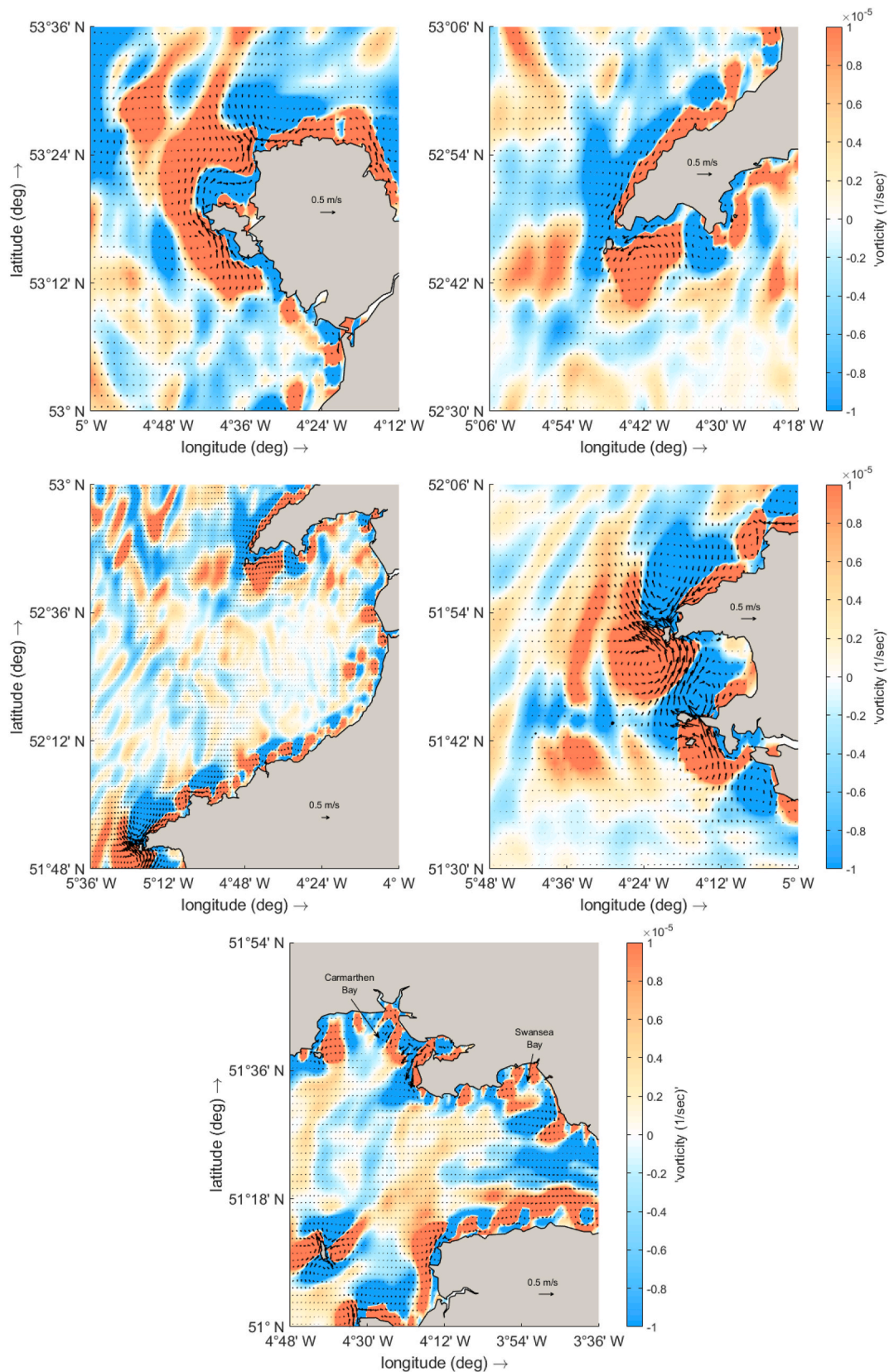


Fig. 12. Computed residual currents (arrows) and contours for the magnitude of the vorticity for a) Anglesey, b) Llyn Peninsula, c) Cardigan Bay, d) Pembrokeshire and e) Carmarthen and Swansea Bays.

Fig. 12c shows the vorticity in Cardigan Bay. A complex structure is present in this area, mostly due to its shallow but highly variable bathymetry. A succession of positive and negative gyres is present in the central and southern part of the bay. Positive vorticity regions coincide with shallow water areas (Sarn Badrig patches, Cynfelyn patches, which are shallow subtidal reefs near the coast of Borth and Aberystwyth - Fig. 11) while negative regions coincide with deeper water areas or deep channels around higher relief seabed features. The largest gyre located in the central part of the bay offshore of Aberystwyth is cyclonic and another cyclonic gyre is apparent in front of Borth, north of Aberystwyth.

In Pembrokeshire (Fig. 12d) there is an area of strong positive vorticity west of Ramsey Island. South of St David's Head a region of negative vorticity is present which continues to the south to St Brides Bay until encountering the anticlockwise gyre towards the west. This is an area where strong currents are present and is a potential site for tidal stream device deployment.

Fig. 12e, shows strong positive vorticity gyres at the south east of Swansea Bay and south east of Carmarthen Bay which coincide with shallow water areas (Scarweather sandbank in Swansea Bay and Nash sandbanks in Carmarthen Bay) and negative vorticity on each side of these sandbanks that coincide with deeper waters.

Coastal features in the area, (such as headlands and sandbanks), produce characteristic gyre patterns of residual tidal flow which are the result of vorticity transfer from the tide to the residual flow (See Figs. 11 and 12). For example, positive and negative gyres are present in front of the east coast of Ireland between Rosslare and Kingstown (See Fig. 3 – No 29 and 3) due to the sandbanks present in the area. Regions of positive vorticity coincide with the locations of sandbanks, (e.g. Lucifer Banks, Wicklow Banks, Kish and Bray Banks), while negative regions coincide with the deeper channels either side of the sandbanks.

Figs. 11 and 12 show that relatively large regions of vorticity of the same sign are often composed of a series of individual gyres with the same rotational sense. Similar observations were found by Robinson (1983) in his study of the Irish Sea and in the study of the Wadden Sea by Ridderinkhof (1989), who attributed the small scale variations in the residual current field to the transfer of vorticity to the time mean or residual flow. This transfer can be most effective in zones where there is a transition from straight to curved depth contours, creating a gradient in the production of vorticity.

The pattern of tidal residuals currents and vorticity has broader potential implications. For example, there are gyres evident in the coastal area between Aberystwyth and Borth in Cardigan Bay. This area is the focal point of converging and diverging currents. An anticlockwise flow pattern occurs in front of the Aberystwyth coast, whereas a clockwise flow pattern appears in the south of the Aberystwyth coast. This area coincides with persistent erosion (Wood, 1971). The pattern of residuals does not prove a link but is suggestive and would indicate beach material disturbed during storms or washed out from the River Dyfi (North of Aberystwyth) on peak ebb tides might be taken offshore by residual currents and lost from the coastal cell, thereby contributing to erosion of the beach.

There is a wide range of tidal residual current magnitude with the strongest found in the Severn Estuary, sandbank areas in front of the Irish Coast (Arklow, Blackwater, Glassgorman Banks), north-west of Anglesey, Llyn Peninsula, in the North Channel and north and south of the Isle of Man, sandbanks in the Bristol Channel (Nash, Helwick, Scarweather Banks). Strong residual currents are found particularly near headlands, and near sandbanks. Areas of weak residual currents are found in the southwest of the Isle of Man, in the middle of the Irish Sea between the Irish coast and Cardigan Bay in Wales, also between the Isle of Man and the Cumbrian coast.

The sandbanks along the Irish east coast are areas identified for the development of offshore windfarms, (Arklow Banks wind farm) and the proposed Kish and Bray Banks wind farm. Knowledge of the residual flows around these areas is important for understanding likely sediment

movements over the operational lifetime of the farms that might affect their stability and exposure to waves and currents. The banks offer coastal protection and they exercise a strong control on the tidal flow pathways near the coast. The residual current on the Arklow sandbank (north of Rosslare), reveals a clockwise circulation along the bank with a residual flow northward on the left side of the bank and a southward direction of the residual flow on the right side of the bank. This residual flow pattern circulation tends to maintain the sediment within the gyre, following the mechanism proposed by Huthnance (1973). Intensive 3-D modelling of residual currents and potential sediment movement may be justified in areas where tidal stream resources are planned, (e.g. Fairley et al., 2015; Chatzirodou et al., 2019).

## 5. Conclusions

A tidal model for the Irish Sea and the Celtic Sea with a resolution of  $\sim 2$  km has been constructed, calibrated and validated against independent data. The model was nested from a coarser, shelf-scale model with a resolution of  $\sim 3.5$  km driven by 13 tidal constituents:  $M_2$ ,  $S_2$ ,  $N_2$ ,  $K_2$ ,  $K_1$ ,  $O_1$ ,  $P_1$ ,  $Q_1$ ,  $MF$ ,  $MM$ ,  $M_4$ ,  $MS_4$  and  $MN_4$ . The validation of the model against independent tidal measurements demonstrated that the model is capable of correctly capturing the barotropic tidal dynamics of the Irish and Celtic Seas. Detailed analyses of tidal characteristics have been presented with discussions on how these may feed into broader considerations of managing the marine environment. The geographical variation in the tidal characteristics around the Welsh shoreline is large. The magnitude and distribution of this variation has implications for future tidal energy developments, coastal protection, flood defence and ecological studies. The findings presented here provide new knowledge required for such studies.

Our most important findings are:

- The South- and North-Wales coastline is largely mega-tidal while the west coast is macro-tidal. The tidal regime is such that tides are semi-diurnal everywhere and the  $M_2$  tidal harmonic predominates;
- A 180-degree phase difference in  $M_2$  and  $S_2$  tidal components exists between the northern Celtic Sea and the middle region of the Irish Sea confirming the picture of a standing wave type tidal motion;
- Estuaries and semi-enclosed nearshore areas around the Welsh coastline experience significant tidal amplification.  $M_4$  is the most significant shallow water harmonic around the Welsh estuarine coast and around the north-east Irish coast where the  $M_2$  harmonic is diminished due to an amphidromic point;
- The generation of  $M_4$  and other overtides and compound harmonics around the Welsh coast means that the tides have a fine spatial structure and are asymmetric;
- The south and north coastlines of Wales are largely flood-dominant while the west coast is ebb dominant;
- The structure of tidal residual currents exhibits a rich pattern of gyres, the strongest of these being closely correlated to the locations of offshore sandbanks. The presence of the largest gyres may be understood from the generation and dissipation of vorticity of the depth-averaged flow.

## Authorship statement

JM Horrillo-Caraballo: Formal analysis, Methodology, Software, Visualization, Writing – original draft. Yunzhu Yin: Writing – review. Iain Fairley: Writing – review & editing. Harshinie Karunaratna: Writing – review & editing. Ian Masters: Writing – review. DE Reeve: Conceptualization, Methodology, Funding acquisition, Project administration, Writing – review & editing.

## Declaration of competing interest

The authors declare that they have no known competing financial

interests or personal relationships that could have appeared to influence the work reported in this paper.

**Acknowledgements**

The authors gratefully acknowledge funding from the European

Regional Development Fund through the Welsh Government via the SEACAMS2 project. HK acknowledges NERC COASTWEB: Valuing the contribution that COASTal habitats make to human health and WELL-Being, with a focus on the alleviation of natural hazards (NE/N013573/1) project.

**APPENDIX A**

**Table A.1**  
Calibration statistics for selected CSM observation points using different Chézy coefficient.

Location	Chézy coefficient (m <sup>1/2</sup> /s)	RMSE (m)	Correlation (r <sup>2</sup> )
32 Douglas	55	0.446	0.979
	65	0.369	0.980
	<b>75</b>	<b>0.341</b>	<b>0.980</b>
	90	0.366	0.979
31 Fishguard	55	0.323	0.986
	65	0.327	0.991
	<b>75</b>	<b>0.339</b>	<b>0.992</b>
	90	0.376	0.988
34 Heysham	55	0.742	0.968
	65	0.568	0.976
	<b>75</b>	<b>0.516</b>	<b>0.977</b>
	90	0.587	0.973
7 Hinkley Point	55	1.012	0.958
	65	0.824	0.970
	<b>75</b>	<b>0.788</b>	<b>0.971</b>
	90	0.957	0.963
24 Holyhead	55	0.175	0.994
	65	0.181	0.994
	<b>75</b>	<b>0.202</b>	<b>0.995</b>
	90	0.239	0.994
40 Lundy Island	55	0.457	0.980
	65	0.481	0.990
	<b>75</b>	<b>0.548</b>	<b>0.995</b>
	90	0.686	0.996

**Table A.2**  
Calibration statistics for selected observation points.

Location	CSM			ICSM		
	RMSE (m)	Correlation Coefficient (r <sup>2</sup> )	Percentage RMSE (%)	RMSE (m)	Correlation Coefficient (r <sup>2</sup> )	Percentage RMSE (%)
32 Douglas	0.341	0.980	5.35	0.322	0.982	4.97
31 Fishguard	0.339	0.992	6.19	0.235	0.994	4.61
34 Heysham	0.516	0.977	5.76	0.506	0.978	5.48
7 Hinkley Point	0.788	0.971	8.36	0.718	0.977	8.54
24 Holyhead	0.202	0.995	3.60	0.192	0.995	3.44
40 Lundy Island	0.548	0.995	6.17	0.437	0.994	5.19

**APPENDIX B**

**Table B1**  
Amplitude (in metres) and phase (in degree) from the IHO tidal stations included in Delft Dashboard (Nederhoff et al., 2016), model results and their difference.

	O <sub>1</sub>		K <sub>1</sub>		N <sub>2</sub>		M <sub>2</sub>		S <sub>2</sub>		M <sub>4</sub>		MS <sub>4</sub>		M <sub>6</sub>	
	A	ph	A	ph	A	ph	A	ph	A	ph	A	ph	A	ph	A	ph
<b>1 HILBRE ISLAND</b>																
Measured	0.113	41.0	0.119	188.0	0.566	295.0	2.974	319.0	0.953	2.0	0.146	213.0	0.085	267.0	0.021	34.0
Model	0.078	70.3	0.063	212.1	0.390	321.9	2.414	344.1	0.654	31.2	0.530	283.4	0.329	332.3	0.133	184.8
Difference	-0.035	29.3	-0.056	24.1	-0.176	26.9	-0.560	25.1	-0.299	29.2	0.384	70.4	0.244	65.3	0.112	150.8

(continued on next page)

Table B1 (continued)

	O <sub>1</sub>		K <sub>1</sub>		N <sub>2</sub>		M <sub>2</sub>		S <sub>2</sub>		M <sub>4</sub>		MS <sub>4</sub>		M <sub>6</sub>	
	A	ph	A	ph	A	ph										
<b>2 KINGSTOWN</b>																
Measured	0.055	55.1	0.045	196.1	0.252	303.3	1.363	325.3	0.404	9.3	0.080	338.5	0.047	276.5	0.016	11.8
Model	0.084	57.6	0.051	187.4	0.222	286.7	1.045	317.1	0.347	344.4	0.094	102.8	0.062	147.1	0.026	171.6
Difference	0.029	2.5	0.006	-8.7	-0.030	-16.6	-0.318	-8.2	-0.057	-24.9	0.014	124.3	0.015	-129.4	0.010	159.8
<b>3 NEWPORT</b>																
Measured	0.080	2.4	0.075	138.7	0.775	185.4	4.133	198.0	1.482	254.8	0.175	357.1	0.150	26.5	0.079	279.0
Model	0.051	50.6	0.043	175.6	0.414	242.7	2.643	261.0	0.736	314.8	0.592	130.7	0.357	182.8	0.149	314.2
Difference	-0.029	48.2	-0.032	36.9	-0.361	57.3	-1.490	63.0	-0.746	60.0	0.417	133.6	0.207	156.3	0.070	35.2
<b>4 MILFORD HAVEN</b>																
Measured	0.067	354.0	0.064	132.1	0.418	152.4	2.230	171.5	0.827	215.6	0.061	306.5	0.029	10.7	0.014	166.6
Model	0.055	12.8	0.048	131.5	0.406	169.8	2.324	188.2	0.747	236.5	0.266	325.7	0.225	14.9	0.117	29.6
Difference	-0.012	18.8	-0.016	-0.6	-0.012	17.4	0.094	16.7	-0.080	20.9	0.205	19.2	0.196	4.2	0.103	-137.0
<b>5 WICKLOW</b>																
Measured	0.084	28.2	0.092	184.0	0.169	272.6	0.835	301.3	0.189	326.7	0.070	341.3	0.026	27.1	0.004	230.6
Model	0.078	56.4	0.047	183.8	0.158	273.1	0.655	304.4	0.262	324.6	0.049	106.9	0.025	148.3	0.014	145.7
Difference	-0.006	28.2	-0.045	-0.2	-0.011	0.5	-0.180	3.1	0.073	-2.1	-0.021	125.6	-0.001	121.2	0.010	-84.9
<b>6 BOSCASTLE</b>																
Measured	0.050	17.1	0.060	113.0	0.460	104.6	2.360	143.0	0.890	201.0	0.130	32.0	0.160	65.0	-	-
Model	0.057	354.1	0.048	110.4	0.523	138.3	2.737	158.6	0.955	202.5	0.056	181.0	0.053	238.4	0.013	252.8
Difference	0.007	-23.0	-0.012	-2.6	0.063	33.7	0.377	15.6	0.065	1.5	-0.074	149.0	-0.107	173.4	-	-
<b>7 HINKLEY POINT</b>																
Measured	0.100	330.0	0.070	105.0	0.780	165.0	3.800	185.0	1.420	237.0	0.120	2.0	0.050	351.0	0.040	222.0
Model	0.055	29.1	0.046	154.5	0.504	202.0	3.199	219.8	0.909	271.5	0.232	356.7	0.214	62.4	0.101	130.1
Difference	-0.045	59.1	-0.024	49.5	-0.276	37.0	-0.601	34.8	-0.511	34.5	0.112	-5.3	0.164	71.4	0.061	-91.9
<b>8 PORT ST MARY</b>																
Measured	0.110	37.1	0.100	191.0	0.360	300.6	1.950	325.0	0.630	3.0	0.020	296.0	0.010	332.0	-	-
Model	0.087	57.2	0.060	191.1	0.337	301.4	1.763	329.1	0.545	7.7	0.047	56.3	0.032	113.5	0.013	44.8
Difference	-0.023	20.1	-0.040	0.1	-0.023	0.8	-0.187	4.1	-0.085	4.7	0.027	120.3	0.022	141.5	-	-
<b>9 NEW BRIGHTON</b>																
Measured	0.118	37.9	0.119	190.5	0.564	294.2	3.060	318.8	0.998	3.7	0.231	198.5	0.143	244.1	0.052	329.4
Model	0.093	61.9	0.071	199.6	0.515	317.4	2.914	337.6	0.892	26.6	0.360	245.2	0.270	292.0	0.070	97.8
Difference	-0.025	24.0	-0.048	9.1	-0.049	23.2	-0.146	18.8	-0.106	22.9	0.129	46.7	0.127	47.9	0.018	128.4
<b>10 SWANSEA</b>																
Measured	0.059	357.1	0.056	127.7	0.592	154.8	3.144	173.1	1.131	220.3	0.055	29.4	0.034	107.4	0.035	9.0
Model	0.054	14.0	0.047	135.2	0.508	168.8	3.034	188.4	0.933	235.3	0.233	310.2	0.228	13.1	0.099	41.8
Difference	-0.005	16.9	-0.009	7.5	-0.084	14.0	-0.110	15.3	-0.198	15.0	0.178	-79.2	0.194	-94.3	0.064	32.8
<b>11 CAERNARVON</b>																
Measured	0.061	57.0	0.140	200.0	0.351	269.0	1.612	292.0	0.533	332.0	0.143	115.0	0.094	170.0	-	-
Model	0.079	38.9	0.055	167.4	0.329	242.2	1.613	266.2	0.591	303.9	0.074	86.2	0.049	114.1	0.025	198.3
Difference	0.018	-18.1	-0.085	-32.6	-0.022	-26.8	0.001	-25.8	0.058	-28.1	-0.069	-28.8	-0.045	-55.9	-	-
<b>12 FORT BELAN</b>																
Measured	0.058	52.0	0.122	182.0	0.290	260.0	1.433	285.0	0.491	320.0	0.104	68.0	0.052	126.0	-	-
Model	0.079	38.9	0.055	167.4	0.329	242.2	1.612	266.2	0.591	303.9	0.074	86.2	0.049	114.0	0.025	198.0
Difference	0.021	-13.1	-0.067	-14.6	0.039	-17.8	0.179	-18.8	0.100	-16.1	-0.030	18.2	-0.003	-12.0	-	-
<b>13 WYLFA HEAD</b>																
Measured	0.104	30.0	0.110	195.0	0.411	276.0	2.067	300.0	0.680	340.0	0.043	182.0	0.021	259.0	-	-
Model	0.088	46.1	0.062	178.3	0.394	277.6	2.046	302.8	0.667	342.3	0.019	23.6	0.015	103.8	0.017	293.3
Difference	-0.016	16.1	-0.048	-16.7	-0.017	1.6	-0.021	2.8	-0.013	2.3	-0.024	-158.4	-0.006	-155.2	-	-
<b>14 CARDIFF/PENARTH</b>																
Measured	0.067	9.0	0.094	147.0	0.442	161.0	4.090	197.0	1.420	245.0	0.107	14.0	0.098	31.0	0.024	262.0
Model	0.048	49.3	0.041	174.2	0.372	233.5	2.306	252.5	0.662	304.2	0.503	128.1	0.281	177.5	0.097	263.7
Difference	-0.019	40.3	-0.053	27.2	-0.070	72.5	-1.784	55.5	-0.758	59.2	0.396	114.1	0.183	146.5	0.073	1.7
<b>15 BARRY</b>																
Measured	0.073	5.0	0.104	141.0	0.594	165.0	3.816	186.0	1.426	238.0	0.122	32.0	0.049	61.0	0.030	255.0
Model	0.061	23.5	0.048	143.7	0.588	200.3	3.384	218.5	1.078	268.9	0.274	298.1	0.216	1.8	0.047	350.9
Difference	-0.012	18.5	-0.056	2.7	-0.006	35.3	-0.432	32.5	-0.348	30.9	0.152	-93.9	0.167	-59.2	0.017	95.9
<b>16 AVONMOUTH</b>																
Measured	0.079	6.5	0.059	134.0	0.733	187.9	4.223	201.9	1.482	260.4	0.340	347.6	0.296	26.8	0.100	280.8

(continued on next page)

Table B1 (continued)

	O <sub>1</sub>		K <sub>1</sub>		N <sub>2</sub>		M <sub>2</sub>		S <sub>2</sub>		M <sub>4</sub>		MS <sub>4</sub>		M <sub>6</sub>	
	A	ph	A	ph	A	ph										
Model	0.052	52.8	0.043	174.3	0.435	244.6	2.791	261.9	0.780	316.9	0.671	131.8	0.419	184.6	0.183	330.3
Difference	-0.027	46.3	-0.016	40.3	-0.298	56.7	-1.432	60.0	-0.702	56.5	0.331	144.2	0.123	157.8	0.083	49.5
<b>17 PORT ERIN</b>																
Measured	0.100	42.0	0.080	181.0	0.330	275.0	1.760	321.0	0.560	359.0	0.010	92.0	-	-	-	-
Model	0.085	55.4	0.059	190.9	0.295	296.1	1.524	325.1	0.462	2.1	0.050	86.9	0.039	135.3	0.007	150.2
Difference	-0.015	13.4	-0.021	9.9	-0.035	21.1	-0.236	4.1	-0.098	3.1	0.040	-5.1	-	-	-	-
<b>18 HESTAN ISLAND</b>																
Measured	0.094	158.0	0.091	189.0	0.530	318.0	2.755	339.0	0.997	20.0	0.119	280.0	0.055	316.0	-	-
Model	0.096	73.2	0.074	210.6	0.476	343.5	2.679	4.6	0.808	55.5	0.231	313.9	0.157	1.2	0.010	321.9
Difference	0.002	-84.8	-0.017	21.6	-0.054	25.5	-0.076	25.6	-0.189	35.5	0.112	33.9	0.102	45.2	-	-
<b>19 WORKINGTON</b>																
Measured	0.088	28.0	0.134	193.0	0.466	308.0	2.743	335.0	0.768	13.0	0.192	269.0	0.082	294.0	-	-
Model	0.096	72.3	0.074	210.0	0.470	341.8	2.638	2.6	0.796	53.7	0.237	310.0	0.159	357.3	0.020	296.4
Difference	0.008	44.3	-0.060	17.0	0.004	33.8	-0.105	27.6	0.028	40.7	0.045	41.0	0.077	63.3	-	-
<b>20 RAMSEY</b>																
Measured	0.061	62.0	0.137	200.0	0.491	310.0	2.624	328.0	0.924	13.0	0.073	237.0	0.070	279.0	-	-
Model	0.090	61.7	0.065	198.0	0.417	316.8	2.246	341.7	0.687	26.0	0.023	50.2	0.021	148.2	0.017	356.8
Difference	0.029	-0.3	-0.072	-2.0	-0.074	6.8	-0.378	13.7	-0.237	13.0	-0.050	173.2	-0.049	-130.8	-	-
<b>21 ILFRACOMBE</b>																
Measured	0.037	329.0	0.046	65.0	0.326	163.0	3.267	166.0	1.122	207.0	0.110	16.0	0.061	45.0	-	-
Model	0.061	0.4	0.049	118.2	0.620	156.9	3.317	176.6	1.150	222.7	0.129	240.2	0.107	302.1	0.017	229.9
Difference	0.024	31.4	0.003	53.2	0.294	-6.1	0.050	10.6	0.028	15.7	0.019	-135.8	0.046	-102.9	-	-
<b>22 APPLIEDORE</b>																
Measured	0.067	358.0	0.067	140.0	0.482	147.0	2.542	165.0	0.920	211.0	0.168	272.0	0.128	315.0	-	-
Model	0.022	63.3	0.020	185.8	0.068	164.6	0.198	192.2	0.147	225.2	0.159	14.0	0.139	48.9	0.091	184.9
Difference	-0.045	65.3	-0.047	45.8	-0.414	17.6	-2.344	27.2	-0.773	14.2	-0.009	102.0	0.011	93.9	-	-
<b>23 LOUGH LARNE</b>																
Measured	0.102	39.2	0.125	172.5	0.179	292.0	0.920	318.4	0.216	355.5	0.023	55.8	0.020	94.4	0.007	207.9
Model	0.077	48.9	0.049	190.8	0.122	282.0	0.597	318.6	0.115	348.3	0.022	261.8	0.010	340.2	0.017	197.5
Difference	-0.025	9.7	-0.076	18.3	-0.057	-10.0	-0.323	0.2	-0.101	-7.2	-0.001	-154.0	-0.010	-114.2	0.010	-10.4
<b>24 HOLYHEAD</b>																
Measured	0.094	34.4	0.107	181.3	0.360	267.3	1.788	291.8	0.591	328.3	0.029	38.7	0.009	105.4	0.023	216.9
Model	0.085	42.5	0.060	173.0	0.354	264.2	1.789	289.5	0.607	327.2	0.046	349.9	0.030	43.7	0.014	251.1
Difference	-0.009	8.1	-0.047	-8.3	-0.006	-3.1	0.001	-2.3	0.016	-1.1	0.017	-48.8	0.021	-61.7	-0.009	34.2
<b>25 AMLWCH</b>																
Measured	0.080	49.0	0.030	189.0	0.450	282.0	2.350	305.0	0.710	341.0	0.060	185.0	0.020	243.0	-	-
Model	0.090	47.2	0.063	179.9	0.424	281.7	2.221	306.7	0.719	347.1	0.013	12.1	0.011	128.4	0.023	310.7
Difference	0.010	-1.8	0.033	-9.1	-0.026	-0.3	-0.129	1.7	0.009	6.1	-0.047	-172.9	-0.009	-114.6	-	-
<b>26 BEAUMARIS</b>																
Measured	0.117	26.8	0.118	192.3	0.505	281.9	2.539	311.7	0.751	350.1	0.136	185.0	0.081	234.1	0.024	5.0
Model	0.094	51.7	0.067	185.4	0.491	293.9	2.610	316.8	0.842	0.6	0.092	155.0	0.085	201.7	0.066	351.0
Difference	-0.023	24.9	-0.051	-6.9	-0.014	12.0	0.071	5.1	0.091	10.5	-0.044	-30.0	0.004	-32.4	0.042	-14.0
<b>27 LLANDUDNO</b>																
Measured	0.113	39.9	0.132	185.2	0.561	294.5	2.672	308.4	0.848	345.5	0.116	181.1	0.074	225.2	0.020	355.9
Model	0.088	52.9	0.064	189.7	0.462	293.0	2.583	316.5	0.806	0.0	0.065	203.6	0.066	244.6	0.072	3.2
Difference	-0.025	13.0	-0.068	4.5	-0.099	-1.5	-0.089	8.1	-0.042	14.5	-0.051	22.5	-0.008	19.4	0.052	7.3
<b>28 TENBY</b>																
Measured	0.100	1.0	0.120	119.0	0.490	155.0	2.620	170.0	1.010	215.0	0.060	293.0	0.010	257.0	-	-
Model	0.053	11.5	0.046	131.1	0.468	162.3	2.724	182.4	0.860	228.0	0.171	329.4	0.173	19.8	0.097	12.2
Difference	-0.047	10.5	-0.074	12.1	-0.022	7.3	0.104	12.4	-0.150	13.0	0.111	36.4	0.163	122.8	-	-
<b>29 ROSSLARE</b>																
Measured	0.073	44.3	0.065	182.6	0.102	140.6	0.562	159.5	0.252	220.9	0.035	51.3	0.012	91.4	0.005	320.4
Model	0.059	49.2	0.035	161.8	0.169	176.3	0.875	186.3	0.355	242.9	0.048	207.7	0.035	269.6	0.019	0.5
Difference	-0.014	4.9	-0.030	-20.8	0.067	35.7	0.313	26.8	0.103	22.0	0.013	156.4	0.023	178.2	0.014	40.1
<b>30 BURRY PORT</b>																
Measured	0.058	355.0	0.055	140.0	0.540	154.0	2.795	175.0	1.033	220.0	0.094	281.0	0.024	298.0	-	-
Model	0.056	19.0	0.047	137.9	0.448	181.8	2.642	199.7	0.815	249.2	0.440	349.2	0.321	40.1	0.061	130.7
Difference	-0.002	24.0	-0.008	-2.1	-0.092	27.8	-0.153	24.7	-0.218	29.2	0.346	68.2	0.297	102.1	-	-

(continued on next page)

**Table B1** (continued)

	K <sub>1</sub>		N <sub>2</sub>		M <sub>2</sub>		S <sub>2</sub>		M <sub>4</sub>		MS <sub>4</sub>		M <sub>6</sub>			
	A	ph	A	ph	A	ph										
<b>31 FISHGUARD</b>																
Measured	0.073	4.0	0.085	158.0	0.299	186.0	1.317	207.0	0.524	247.0	0.104	16.0	0.055	62.0	–	–
Model	0.068	21.8	0.050	142.2	0.347	190.0	1.730	210.1	0.652	253.4	0.024	155.0	0.017	280.2	0.007	90.9
Difference	–0.005	17.8	–0.035	–15.8	0.048	4.0	0.413	3.1	0.128	6.4	–0.080	139.0	–0.038	–141.8	–	–
<b>32 DOUGLAS</b>																
Measured	0.159	38.0	0.098	181.0	0.472	301.0	2.274	326.0	0.756	9.0	0.049	226.0	0.055	232.0	–	–
Model	0.089	60.2	0.063	195.2	0.393	310.5	2.096	336.5	0.647	18.2	0.044	52.1	0.029	119.9	0.022	9.9
Difference	–0.070	22.2	–0.035	14.2	–0.079	9.5	–0.178	10.5	–0.109	9.2	–0.005	–173.9	–0.026	–112.1	–	–
<b>33 CARRICKFERGUS</b>																
Measured	0.073	32.0	–	–	0.219	295.0	1.143	317.0	0.320	352.0	0.003	277.0	0.009	175.0	–	–
Model	0.077	49.1	0.049	190.9	0.119	282.3	0.582	319.1	0.110	349.2	0.024	256.6	0.010	328.9	0.017	196.8
Difference	0.004	17.1	–	–	–0.100	–12.7	–0.561	2.1	–0.210	–2.8	0.021	–20.4	0.001	153.9	–	–
<b>34 HEYSHAM</b>																
Measured	0.104	3.0	0.116	185.0	0.619	310.0	3.274	328.0	1.155	6.0	0.128	265.0	0.122	298.0	–	–
Model	0.097	66.6	0.075	203.4	0.533	330.2	2.994	349.9	0.920	40.5	0.366	276.1	0.270	325.2	0.035	157.1
Difference	–0.007	63.6	–0.041	18.4	–0.086	20.2	–0.280	21.9	–0.235	34.5	0.238	11.1	0.148	27.2	–	–
<b>35 PORTHCAWL</b>																
Measured	0.030	343.0	0.091	123.0	0.639	153.0	3.170	173.0	1.249	228.0	0.122	9.0	0.030	65.0	–	–
Model	0.054	15.4	0.046	137.2	0.510	172.8	3.074	192.4	0.936	239.7	0.200	318.5	0.207	21.8	0.097	56.6
Difference	0.024	32.4	–0.045	14.2	–0.129	19.8	–0.096	19.4	–0.313	11.7	0.078	–50.5	0.177	–43.2	–	–
<b>36 WESTON-SUPER-MARE</b>																
Measured	0.064	358.0	0.082	113.0	0.533	245.0	4.432	195.0	1.430	245.0	0.119	33.0	0.073	35.0	–	–
Model	0.059	31.8	0.047	155.2	0.529	215.1	3.226	232.0	0.961	285.1	0.314	355.8	0.255	55.5	0.117	69.0
Difference	–0.005	33.8	–0.035	42.2	–0.004	–29.9	–1.206	37.0	–0.469	40.1	0.195	–37.2	0.182	20.5	–	–
<b>37 WATCHET</b>																
Measured	0.064	24.0	0.098	132.0	0.905	165.0	3.063	175.0	1.703	232.0	0.125	52.0	0.043	33.0	–	–
Model	0.063	17.2	0.049	138.4	0.629	190.2	3.598	207.8	1.165	258.3	0.371	290.0	0.287	351.5	0.061	330.2
Difference	–0.001	–6.8	–0.049	6.4	–0.276	25.2	0.535	32.8	–0.538	26.3	0.246	–122.0	0.244	–41.5	–	–
<b>38 PORT TALBOT</b>																
Measured	0.080	6.0	0.080	136.0	0.570	153.0	3.150	173.0	1.150	220.0	0.050	26.0	0.030	106.0	0.030	23.0
Model	0.052	16.9	0.045	139.2	0.466	167.5	2.853	187.7	0.847	233.9	0.268	331.9	0.258	27.5	0.131	44.0
Difference	–0.028	10.9	–0.035	3.2	–0.104	14.5	–0.297	14.7	–0.303	13.9	0.218	–54.1	0.228	–78.5	0.101	21.0
<b>39 BARROW-IN-FURNESS</b>																
Measured	0.110	47.0	0.120	193.0	0.580	307.0	3.080	331.0	1.000	15.0	0.190	252.0	0.120	296.0	0.030	49.0
Model	0.097	67.0	0.075	203.3	0.532	331.2	2.988	350.8	0.917	41.5	0.370	278.9	0.271	328.0	0.039	163.3
Difference	–0.013	20.0	–0.045	10.3	–0.048	24.2	–0.092	19.8	–0.083	26.5	0.180	26.9	0.151	32.0	0.009	114.3
<b>40 LUNDY ISLAND</b>																
Measured	0.050	350.0	0.080	122.0	0.470	144.0	2.340	164.0	0.820	209.0	0.060	314.0	0.030	7.0	0.030	143.0
Model	0.050	358.5	0.048	115.0	0.546	149.6	2.860	169.9	1.003	214.6	0.056	241.2	0.055	296.0	0.010	303.7
Difference	0.000	8.5	–0.032	–7.0	0.076	5.6	0.520	5.9	0.183	5.6	–0.004	–72.8	0.025	–71.0	–0.020	160.7
<b>41 ABERDOVEY</b>																
Measured	0.120	356.0	0.050	165.0	0.270	225.0	1.450	237.0	0.570	276.0	0.190	59.0	0.100	111.0	0.010	118.0
Model	0.074	28.5	0.053	153.6	0.387	209.5	1.908	229.5	0.737	272.5	0.051	117.8	0.019	41.3	0.040	224.6
Difference	–0.046	32.5	0.003	–11.4	0.117	–15.5	0.458	–7.5	0.167	–3.5	–0.139	58.8	–0.081	–69.7	0.030	106.6
<b>42 PORTPATRICK</b>																
Measured	0.100	42.0	0.110	190.0	0.260	306.0	1.340	333.0	0.380	16.0	0.010	277.0	0.010	107.0	–	–
Model	0.081	56.6	0.056	196.0	0.192	307.8	1.005	340.4	0.262	21.0	0.012	236.0	0.004	241.9	0.012	176.2
Difference	–0.019	14.6	–0.054	6.0	–0.068	1.8	–0.335	7.4	–0.118	5.0	0.002	–41.0	–0.006	134.9	–	–
<b>43 WELLHOUSE ROCK</b>																
Measured	0.030	42.0	0.090	89.0	0.430	212.0	2.680	237.0	0.880	296.0	0.820	83.0	0.630	135.0	0.130	285.0
Model	0.040	56.5	0.035	176.5	0.327	239.4	1.883	258.2	0.600	309.9	0.827	148.5	0.480	199.5	0.231	11.0
Difference	0.010	14.5	–0.055	87.5	–0.103	27.4	–0.797	21.2	–0.280	13.9	0.007	65.5	–0.150	64.5	0.101	86.0
<b>44 BERKELEY</b>																
Measured	0.090	357.0	0.040	159.0	0.440	205.0	3.010	234.0	0.940	303.0	0.800	65.0	0.690	133.0	0.110	257.0
Model	0.059	48.1	0.047	170.1	0.515	248.2	3.289	264.5	0.924	320.9	0.713	108.9	0.483	164.2	0.061	337.3
Difference	–0.031	51.1	0.007	11.1	0.075	43.2	0.279	30.5	–0.016	17.9	–0.087	43.9	–0.207	31.2	–0.049	80.3
<b>45 WHITE HOUSE</b>																
Measured	0.120	0.0	0.070	131.0	0.490	195.0	3.540	224.0	1.140	287.0	0.630	53.0	0.550	96.0	0.110	280.0
Model	0.058	47.5	0.047	170.5	0.512	247.9	3.274	264.3	0.920	320.6	0.699	108.7	0.473	163.9	0.060	340.4

(continued on next page)

Table B1 (continued)

	O <sub>1</sub>		K <sub>1</sub>		N <sub>2</sub>		M <sub>2</sub>		S <sub>2</sub>		M <sub>4</sub>		MS <sub>4</sub>		M <sub>6</sub>	
	A	ph	A	ph	A	ph										
<i>Difference</i>	-0.062	47.5	-0.023	39.5	0.022	52.9	-0.266	40.3	-0.220	33.6	0.069	55.7	-0.077	67.9	-0.050	60.4
<b>46 INWARD ROCKS</b>																
Measured	0.080	3.0	0.040	135.0	0.610	208.0	3.940	223.0	1.260	290.0	0.520	21.0	0.500	85.0	0.090	312.0
Model	0.058	47.2	0.047	170.6	0.510	247.8	3.263	264.2	0.917	320.5	0.687	108.6	0.465	163.8	0.057	341.3
<i>Difference</i>	-0.022	44.2	0.007	35.6	-0.100	39.8	-0.677	41.2	-0.343	30.5	0.167	87.6	-0.035	78.8	-0.033	29.3
<b>47 AUST</b>																
Measured	0.090	345.0	0.030	161.0	0.530	188.0	4.150	210.0	1.340	272.0	0.390	358.0	0.450	52.0	0.070	304.0
Model	0.058	47.0	0.047	170.8	0.508	247.9	3.246	264.2	0.911	320.6	0.675	108.6	0.456	163.9	0.056	341.5
<i>Difference</i>	-0.032	62.0	0.017	9.8	-0.022	59.9	-0.904	54.2	-0.429	48.6	0.285	110.6	0.006	111.9	-0.014	37.5
<b>48 ISLE OF WHITHORN</b>																
Measured	0.120	62.0	0.160	178.0	0.380	309.0	2.360	334.0	0.730	19.0	0.100	255.0	0.070	309.0	0.010	123.0
Model	0.091	65.6	0.067	202.1	0.422	327.1	2.292	352.7	0.699	37.7	0.058	5.2	0.028	69.3	0.012	133.7
<i>Difference</i>	-0.029	3.6	-0.093	24.1	0.042	18.1	-0.068	18.7	-0.031	18.7	-0.042	110.2	-0.042	120.3	0.002	10.7
<b>49 DRUMMORE</b>																
Measured	0.100	46.0	0.111	189.0	0.340	310.0	2.020	337.0	0.670	21.0	0.050	253.0	0.050	281.0	0.010	176.0
Model	0.088	64.3	0.063	201.2	0.323	325.1	1.739	353.0	0.511	36.4	0.047	22.2	0.027	85.2	0.024	184.5
<i>Difference</i>	-0.012	18.3	-0.048	12.2	-0.017	15.1	-0.281	16.0	-0.159	15.4	-0.003	129.2	-0.023	164.2	0.014	8.5
<i>Average</i>	-0.013	20.1	-0.036	11.6	-0.053	16.4	-0.280	17.7	-0.174	16.9	0.081	21.5	0.055	22.9	0.030	41.2
<i>RMSE</i>	0.026	32.3	0.045	24.8	0.130	28.0	0.637	25.7	0.298	25.5	0.161	96.8	0.124	101.1	0.041	61.8

## References

- Adcock, T.A.A., Draper, S., 2014. Power extraction from tidal channels – multiple tidal constituents, compound tides and overtides. *Renew. Energy* 63, 797–806. <https://doi.org/10.1016/j.renene.2013.10.037>.
- Aldridge, J.N., Davies, A.M., 1993. A high resolution three-dimensional hydrodynamic tidal model of the Eastern Irish Sea. *J. Phys. Oceanogr.* 23, 207–224.
- Amante, C., Eakins, B.W., 2009. ETOPO1 1 arc-minute global relief model: procedures, data sources and analysis. NOAA Technical Memorandum NESDIS NGDC-24. National Geophysical Data Center, NOAA. <https://doi.org/10.7289/V5C8276M> [June 2017].
- Andersen, O.B., 1999. Shallow water tides in the northwest European shelf region from TOPEX/POSEIDON altimetry. *J. Geophys. Res.* 104, 7729–7741.
- Aubrey, D.G., Speer, P.E., 1985. A study of non-linear tidal propagation in shallow inlet/estuarine systems. Part I: Observations. *Estuar. Coast Shelf Sci.* 21, 185–205.
- Bowden, K.F., 1980. Physical and dynamical oceanography of the Irish sea. In: Banner, F. T., Collins, M.B., Massie, K.S. (Eds.), *The North-West European Shelf Seas: The Sea Bed and the Sea in Motion II. Physical and Chemical Oceanography, and Physical Resources*, Elsevier Oceanography Series, vol. 24. Elsevier Scientific Publishing Company, Amsterdam, pp. 391–413. Part B.
- Bryden, I.G., Couch, S.J., 2006. ME1—marine energy extraction: tidal resource analysis. *Renew. Energy* 31 (2), 133–139. <https://doi.org/10.1016/j.renene.2005.08.012>.
- Brown, J.M., Amoudry, L.O., Souza, A.J., Plater, A.J., 2015. Residual circulation modelled at national UK scale to identify sediment pathways to inform coastal evolution models. In: Wang, P., Rosati, J.D., Cheng, J. (Eds.), *The Proceedings of the Coastal Sediments 2015*. World Scientific, Singapore. [https://doi.org/10.1142/9789814689977\\_0137](https://doi.org/10.1142/9789814689977_0137).
- Chatzirodou, A., Karunaratna, H., Reeve, D.E., 2017. Modelling 3D hydrodynamics governing island-associated sandbanks in a proposed tidal stream energy site. *Appl. Ocean Res.* 66, 79–94.
- Chatzirodou, A., Karunaratna, H., Reeve, D.E., 2019. 3D modelling of the impacts of in-stream horizontal-axis tidal energy converters (TECs) on offshore sandbank dynamics. *Appl. Ocean Res.* 91, 101882.
- Cooper, L.H.N., 1967. The physical oceanography of the Celtic Sea. *Oceanogr. Mar. Biol. Rev.* 5, 99–110.
- Cummins, P.F., Oey, L.Y., 1997. Simulation of barotropic and baroclinic tides off Northern British Columbia. *J. Phys. Oceanogr.* 27, 762–781.
- Davies, J.L., 1964. A morphogenic approach to world shorelines. *Zeit. f. Geomorph.* 8, 27–42.
- Davies, A.M., 1986. A three-dimensional model of the northwest European shelf with application to the M4 tide. *J. Phys. Oceanogr.* 16, 797–813.
- Davies, A.M., Aldridge, J.N., 1993. A numerical model study of parameters influencing tidal currents in the Irish sea. *J. Geophys. Res.* 98 (C4), 7049–7067.
- Davies, A.M., Jones, J.E., 1992. A three-dimensional model of the M<sub>2</sub>, S<sub>2</sub>, N<sub>2</sub>, K<sub>1</sub> and O<sub>1</sub> tides in the Celtic and Irish Sea. *Prog. Oceanogr.* 29, 197–234.
- De Swart, H.E., Zimmerman, J.T.F., 2009. Morphodynamics of tidal inlet systems. *Annu. Rev. Fluid Mech.* 41, 203–229.
- Doodson, A.T., Corkan, R.H., 1932. The principal constituent of the tides in the English and Irish Channels. *Phil. Trans. Roy. Soc. Lond.* 231, 29–53.
- Doodson, A.T., Rossiter, J.R., Corkan, R.H., 1954. Tidal charts based on coastal data: Irish Sea. *Proc. R. Soc. Edinb. Sect. A (Math. Phys. Sci.)* 64, 90–111.
- Egbert, G.D., Erofeeva, S.Y., 2002. Efficient inverse modeling of barotropic ocean tides. *J. Atmos. Ocean. Technol.* 19 (2), 183–204.
- EMODnet Bathymetry Consortium – Emodnet, 2016. EMODnet Digital Bathymetry (DTM). <https://doi.org/10.12770/c7b53704-999d-4721-b1a3-04ec60c87238>. (Accessed October 2016).
- Environment Agency, 2021. What Is Coastal Squeeze? Project FRS17187. Environment Agency, Bristol, UK, p. 238pp.
- Fairley, I., Masters, I., Karunaratna, H., 2015. The cumulative impact of tidal stream turbine arrays on sediment transport in the Pentland Firth. *Renew. Energy* 80, 755–769.
- Flather, R.A., 1976. A tidal model of the north west European Continental Shelf. *Memoires Societe Royale des Sciences de Liege, Ser. 6 (1)*, p141–164.
- Friedrichs, C.T., Aubrey, D.G., 1988. Non-linear tidal distortion in shallow well-mixed estuaries: a synthesis. *Estuarine, Coastal and Shelf Science* 27, 521–545.
- Friedrichs, C.T., Aubrey, D.G., 1994. Tidal propagation in strongly convergent channels. *J. Geophys. Res.* 99 (C2), 3321–3336.
- Gao, C., Adcock, T.A., 2017. On the resonance of the Bristol Channel. *Int. J. Offshore Polar Eng.* 27, p177–183.
- Gallo, M.N., Vinzon, S.B., 2005. Generation of overtides and compound tides in Amazon estuary. *Ocean Dynam.* 55, 441–448.
- Gekeler, J., 1995. Assimilating data into a tidal model of the Irish and Celtic Sea. *Continent. Shelf Res.* 15 (11–12), 1381–1408.
- Horrillo-Caraballo, J.M., Reeve, D.E., 2008. Morphodynamic behaviour of a nearshore sandbank system: the Great Yarmouth Sandbanks, U.K. *Mar. Geol.* 254 (1–2), 91–106. <https://doi.org/10.1016/j.margeo.2008.05.014>.
- Howarth, M.J., 1990. Atlas of Tidal Elevations and Currents Around the British Isles, vol. 293. Department of Energy, London, p. 16. Offshore Technology Report OTH89.
- Howarth, M.J., 2005. Hydrography of the Irish Sea. In: SEA6 Technical Report. UK Department of Trade and Industry's offshore energy - Strategic Environmental Assessment programme, 30pp.
- Hulscher, J.M.H., de Swart, H.E., de Vriend, H.J., 1993. The generation of offshore tidal sand banks and sandwaves. *Continent. Shelf Res.* 13 (11), p1183–1204.
- Huntley, D.A., 1980. Tides on the north-west European continental shelf. In: Banner, F. T., Collins, M.B., Massie, K.S. (Eds.), *The North-West European Shelf Seas: The Sea Bed and the Sea in Motion II. Physical and Chemical Oceanography, and Physical Resources*, Elsevier Oceanography Series, vol. 24. Elsevier Scientific Publishing Company, Amsterdam, pp. 301–351. Part B.
- Huthnance, J.M., 1973. Tidal current asymmetries over the Norfolk sandbanks. *Estuar. Coast Mar. Sci.* 1, 89–99.
- Huthnance, J.M., 1982. On one mechanism forming linear sand banks. *Estuar. Coast Shelf Sci.* 14, 79–99.
- Ianniello, J.P., 1979. Tidally-induced currents in estuaries of variable breadth and depth. *J. Phys. Oceanogr.* 9 (5), p962–974.
- International Council for the Exploration of the Sea – ICES, 2018. Celtic seas ecoregion – ecosystem overview. <https://doi.org/10.17895/ices.pub.4667>.
- Jay, D.A., 1991. Green's law revisited: tidal long-wave propagation in channels with strong topography. *J. Geophys. Res.* 96, 20585–20598.

- Jones, J.E., Davies, A.M., 1996. A high-resolution, three-dimensional model of the  $M_2$ ,  $M_4$ ,  $M_6$ ,  $S_2$ ,  $N_2$ ,  $K_1$  and  $O_1$  tides in the eastern Irish sea. *Estuarine, Coastal and Shelf Science* 42, 311–346.
- Jones, J.E., Davies, A.M., 2007. A high-resolution finite element model of the  $M_2$ ,  $M_4$ ,  $M_6$ ,  $S_2$ ,  $N_2$ ,  $K_1$  and  $O_1$  tides off the west coast of Britain. *Ocean Model.* 19, 70–100.
- Kang, S.K., Lee, S.R., Lie, H.J., 1998. Fine-grid tidal modelling of the Yellow and East China seas. *Continental Shelf Res.* 18, 739–772.
- Lavelle, J.W., Mojfeld, H.O., Baker, E.T., 1984. An in-situ erosion rate for a fine-grained marine sediment. *J. Geophys. Res.* 89 (4), 6543–6552.
- Lesser, G.R., Roelvink, J.A., van Kester, J.A.T.M., Stelling, G.S., 2004. Development and validation of a three-dimensional morphological model. *Coastal Engineering* 51 (8–9), 883–915.
- Levoy, F., Anthony, E.J., Monfort, O., Larsson, C., 2000. The morphodynamics of megatidal beaches in Normandy, France. *Mar. Geol.* 171, 39–59.
- McCave, I.N., 1970. Sand waves in the north sea off the coast of holland. *Mar. Geol.* 10, p199–225.
- Moore, R.D., Wolf, J., Souza, A.J., Flint, S.S., 2009. Morphological evolution of the dee estuary, eastern Irish sea, UK: a tidal asymmetry approach. *Geomorphology* 103, 588–596. <https://doi.org/10.1016/j.geomorph.2008.08.003>.
- Mungall, J.C.H., Matthews, J.B., 1978. The  $M_2$  tide of the Irish sea: hourly configurations of the sea surface and of the depth-mean currents. *Estuar. Coast Mar. Sci.* 6, 55–74.
- Nederhoff, K., van Dongeren, A., van Ormondt, M., 2016. Delft Dashboard: a MATLAB-based rapid tool for setting up coastal and estuarine models. Tool description and model verification 64. Version: 02.02.13278, October 2016, Delft, The Netherlands.
- Neill, S.P., 2009. The role of Coriolis in sandbank formation due to a headland/island system. *Estuar. Coast Shelf Sci.* 79, 419–428.
- Neill, S.P., Litta, E.J., Couch, S.J., Davies, A.G., 2009. The impact of tidal stream turbines on large-scale sediment dynamics. *Renew. Energy* 34, 2803–2812.
- Neill, S.P., Jordan, J.R., Couch, S.J., 2012. Impact of tidal energy converter (TEC) arrays on the dynamics of headland sand banks. *Renew. Energy* 37, 387–397.
- Neill, S.P., Reza Hashemi, M., Lewis, M.J., 2014. The role of tidal asymmetry in characterizing the tidal energy resource of Orkney. *Renew. Energy* 68, 337–350.
- Neill, S.P., Angeloudis, A., Robins, P.E., Walkington, I., Ward, S.L., Masters, I., Lewis, M. J., Piano, M., Avdis, A., Piggott, M.D., 2018. Tidal range energy resource and optimization – past perspectives and future challenges. *Renew. Energy* 127, 763–778.
- Nihoul, J.C.J., Rondonay, F.C., 1975. The influence of the “tidal stress” on the residual circulation. Application to the southern bight of the North Sea. *Tellus* 27 (5), 484–489.
- Ozer, J., Legrand, S., 2015. BEAWAREII: Review of the Physical Oceanography in the Area of the Bonn Agreement. RBINS/OD Nature/MUMM, p. 28.
- Pingree, R.D., 1978. The formation of the Shambles and other banks by tidal stirring of the seas. *J. Mar. Biol. Assoc. U. K.* 58, 211–226.
- Pingree, R.D., 1980. Physical oceanography of the Celtic Sea and English channel. In: Banner, F.T., Collins, M.B., Massie, K.S. (Eds.), *The North-West European Shelf Seas: the Sea Bed and the Sea in Motion II. Physical and Chemical Oceanography, and Physical Resources*, Elsevier Oceanography Series, vol. 24. Elsevier Scientific Publishing Company, Amsterdam, pp. 415–465, 0422-9894, Part B.
- Pingree, R.D., Griffiths, D.K., 1979. Sand transport paths around the British Isles resulting from the  $M_2$  and  $M_4$  tidal interactions. *Journal of the Marine Biology Association UK* 59, 497–513.
- Pingree, R.D., Griffiths, D.K., 1987. Tidal friction for semi-diurnal tides. *Continental Shelf Res.* 7, 1181–1209.
- Prandle, D., 1978. Residual flows and elevations in the southern North Sea. *Proc. Roy. Soc. Lond. A* 359 (1697), p187–228.
- Prandle, D., 1984. A modelling study of the mixing of  $^{137}\text{Cs}$  in the seas of the European continental shelf. *Phil. Trans. Roy. Soc. Lond.* 310, 407–436.
- Prandle, D., 2009. *Estuaries: Dynamics, Mixing, Sedimentation and Morphology*. CUP, UK, p. 236pp.
- Prandle, D., Ryder, D.K., 1989. Comparison of observed (HF radar) and modelled nearshore velocities. *Continental Shelf Res.* 9 (11), 941–963.
- Pugh, D.T., 1981. Tidal amphidrome movement and energy dissipation in the Irish Sea. *G.J.R.astr. Soc.* 67, p515–527.
- Pugh, D.T., Woodworth, P., 2014. *Sea-Level Science: Understanding Tides, Surges, Tsunamis and Mean Sea Level*, 409pp. Cambridge University Press, Cambridge, ISBN 978-1-107-02819-7.
- Ramster, J.W., Hill, H.W., 1969. Current system in the northern Irish sea. *Nature* 224 (5214), 59–61. <https://doi.org/10.1038/224059a0>.
- Ridderinkhof, H., 1989. Tidal and residual flows in the western Dutch Wadden Sea III: vorticity balances. *Neth. J. Sea Res.* 24 (1), 9–26.
- Robinson, I.S., 1979. The tidal dynamics of the Irish and Celtic Seas. *Geophys. J. Int.* 56 (1), 159–197. <https://doi.org/10.1111/j.1365-246X.1979.tb04774.x>.
- Robinson, I.S., 1983. Tidally induced residual flows. In: Johns, B. (Ed.), *Physical Oceanography of Coastal and Shelf Seas*. Elsevier, Amsterdam, pp. 321–356.
- Shapiro, G.I., 2011. Effect of tidal stream power generation on the region-wide circulation in a shallow area. *Ocean Sci.* 7, 165–174.
- Song, D., Wang, X.H., Kiss, A.E., Bao, X., 2011. The contribution to tidal asymmetry by different combinations of tidal constituents. *J. Geophys. Res.* 116, C12007.
- Taylor, G.I., 1919. Tidal friction in the Irish sea. *Philos. Trans. R. Soc. London, Ser. A* 220, 1–33.
- Uncles, R.J., Stephens, J.A., 2007. SEA 8 Technical Report – Hydrography. UK Department of Trade and Industry’s offshore energy - Strategic Environmental Assessment programme, 105pp.
- Van Rijn, L.C., 1993. *Principles of Sediment Transport in Rivers, Estuaries and Coastal Seas*. Aqua Publications, Amsterdam.
- Ward, S.L., Robins, P.E., Lewis, M.J., Iglesias, G., Reza Hashemi, M., Neill, S.P., 2018. Tidal stream resource characterisation in progressive versus standing wave systems. *Appl. Energy* 220, 274–285.
- Weatherall, P., Marks, K.M., Jakobsson, M., Schmitt, T., Tani, S., Arndt, J.E., Rovere, M., Chayes, D., Ferrini, V., Wigley, R., 2015. A new digital bathymetric model of the world’s oceans. *Earth and Space Science* 2 (8), 331–345. <https://doi.org/10.1002/2015EA000107>.
- Welsh Government, 2019. *Wales National Marine Plan*, vol. 180, ISBN 978-1-83876-634-4.
- Williams, M.E., Amoudry, L.O., Brown, J.M., Thompson, C.E.L., 2019. Fine particle retention and deposition in regions of cyclonic tidal current rotation. *Mar. Geol.* 410, 122–134. <https://doi.org/10.1016/j.margeo.2019.01.006>.
- Willis, M., Masters, I., Thomas, S., Gallie, R., Loman, J., Cook, A., Ahmadian, R., Falconer, R., Lin, B., Gao, G., 2010. Tidal turbine deployment in the Bristol Channel: a case study. *Proceedings of the Institution of Civil Engineers – Energy* 163 (3), 93–105.
- Yang, Z., Wang, T., 2013. Tidal residual eddies and their effect on water exchange in Puget Sound. *Ocean Dynam.* 63, 995–1009. <https://doi.org/10.1007/s10236-013-0635-z>.
- Zhou, J., Pan, S., Falconer, R.A., 2014. Effects of open boundary location on the far-field hydrodynamics of a Severn Barrage. *Ocean Model.* 73, 19–29.
- Zimmerman, J.T.F., 1978. Topographic generation of residual circulation by oscillatory tidal currents. *Geophys. Astrophys. Fluid Dynam.* 11, 35–47.
- Zimmerman, J.T.F., 1981. Dynamics, diffusion and geomorphological significance of tidal residual eddies. *Nature* 290, 549–555.